Title

Direct Anodic Oxidation of Methanol on Supported Platinum/Ruthenium Catalyst in Aqueous Cesium Carbonate

Authors

Rauhe, B.R.
McLarnon, F.R.
Cairns, E.J.

Publication Date

1992-07-01

LBL-32137
UC-331

Lawrence Berkeley Laboratory

UNIVERSITY OF CALIFORNIA

ENERGY & ENVIRONMENT DIVISION

Direct Anodic Oxidation of Methanol on Supported Platinum/Ruthenium Catalyst in Aqueous Cesium Carbonate

B.R. Rauhe Jr.*, F.R. McLarnon, and E.J. Cairns
*(M.S Thesis)

July 1992

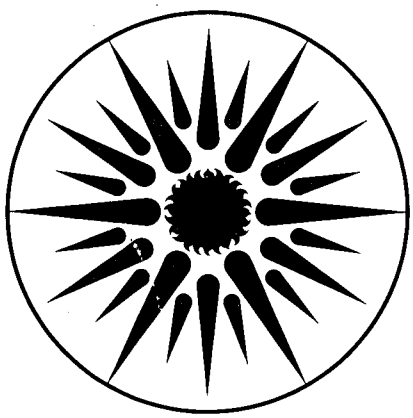

ENERGY & ENVIRONMENT DIVISION

Prepared for the U.S. Department of Energy under Contract Number DE-AC03-76SF00098

DISCLAIMER

LBL-32137

DIRECT ANODIC OXIDATION OF METHANOL ON SUPPORTED PLATINUM/RUTHENIUM CATALYST IN AQUEOUS CESIUM CARBONATE

by

Bruce R. Rauhe, Jr., Frank R. McLarnon and Elton J. Cairns

Energy & Environment Division
Lawrence Berkeley Laboratory
University of California
Berkeley, California 94720

This work was supported by the Assistant Secretary for Conservation and Renewable Energy, Office of Transportation Technologies, Electric and Hybrid Propulsion Division of the U.S. Department of Energy under Contract No. DE-AC03-76SF00098.

Table of Contents

Table of Contents iii

List of Figures v

List of Tables vii

Symbols viii

Acknowledgments x

Chapter 1. Introduction 1

Fuel Cells for Electric Vehicles 1

Methanol Fuel Cells 3

Organization of Thesis 4

Chapter 2. Background 6

Direct Oxidation of Methanol in Aqueous Electrolytes 6

Gas Diffusion Electrodes 9

Methanol Oxidation on Platinum and Platinum-Based Co-catalysts 12

Chapter 3. Experimental Procedures 20

Introduction 20

Electrode Fabrication 22

Cell Performance Studies 28

Chapter 4. Results and Discussion 40

Characterization of catalyst 40

Methanol Oxidation on Platinum/Ruthenium 54

Chapter 5. Conclusions and Recommendations 66

References 69

Appendix A. Electrode Parameters.....78
Appendix B. Fabrication of the Gas Diffusion Electrode.....80

List of Figures

Figure 3-1. Catalyst preparation procedure 24
Figure 3-2. Raman line intensities as function of graphite crystallite size. 26
Figure 3-3. Raman spectrum of graphitized Vulcan XC-72R. 26
Figure 3-4. Teflon half-cell cross section 30
Figure 3-5. Photograph of cell parts 31
Figure 3-6. Exploded view of working electrode and gaskets 32
Figure 3-7. Arrangement of thermostatic oven and cell components 35
Figure 4-1. Lattice parameters of Pt-Ru alloys as determined by XRD. 41
Figure 4-2. XRD of supported Pt-Ru (50:50) catalyst: Pt line 43
Figure 4-3. XRD of supported Pt-Ru (50:50) catalyst: Ru line 43
Figure 4-4. Comparison of cyclic voltammetry on Pt-Ru found in the literature 46
Figure 4-5. Effect of cycling to 1000 mV vs. 1500 mV 48
Figure 4-6. Comparison of degree of wetting for gas diffusion electrodes 49
Figure 4-7. Determination of catalyst surface area 51
Figure 4-8. IR-drop experiment 53
Figure 4-9. Methanol oxidation performance on Pt vs. Pt-Ru 55
Figure 4-10. Comparison of performance for methanol oxidation in this work to literature 57

Figure 4-11. Performance curve at several temperatures used to determine the activation energy for methanol oxidation on Pt-Ru 59
Figure 4-12. Activation energy for methanol oxidation on Pt-Ru 59
Figure 4-13. Performance at several temperatures for 20 and 40 w/o PTFE 61
Figure 4-14. Performance at 120 and 130 °C for various PTFE contents in the reaction layer 63
Figure 4-15. Current density vs. PTFE content in reaction layer at 120 and 130 °C 64
Figure B-1. Vacuum table assembly for adding the reaction layer to the gas diffusion layer 85
Figure B-2. Assembly order for pressing the electrode 86

List of Tables

Table 2-1. References for studies of Pt-based co-catalysts 17

Table 3-1. Physical properties of graphite paper in gas diffusion layer.....23

Table A-1. Parameters for the fabrication of gas diffusion electrodes 79

Table B-1. Parameters for the pressing and sintering the gas diffusion electrode 85

Symbols

A	area (cm^2)
ΔG^o	standard Gibbs free energy (J/mol)
E	reversible potential (mV vs. RHE)
E_A	activation energy, (J/mol)
E^o	standard potential (mV vs. RHE)
F	Faraday's constant (96487 coulombs/equivalent)
i	current density (mA/cm^2)
M	molarity (g-mole/liter)
R	universal gas constant (8.314 J/mol-K)
T	temperature (°C)
W	weight (mg)

Subscripts

adj	adjusted value
cat	catalyst
elec	electrode
f	final
FEP	fluorinated ethylenepropylene
meas	measured value

Superscripts

i	initial
H_2	hydrogen fuel
x	some current value of interest

Acronyms

BET	Brunauer-Emmett-Teller, method for determining surface area by nitrogen adsorptioin
CV	cyclic voltammogram
DEMS	differential electrochemical mass spectroscopy
DI	de-ionized water
ECTDMS	electrochemical thermal differential mass spectroscopy
ESR	electron spin resonance
EV	electric vehicle
EXAFS	extended x-ray absorbance fine structure
FEP	fluorinated ethylenepropylene
GDE	gas diffusion electrode
GDL	gas diffusion layer
LRS	laser Raman spectroscopy
PEM	polymer electrolyte membrane
PTFE	polytetrafluoroethylene
RL	reaction layer
SNIFTIRS	subtractively normalized interference fourier transform infrared spectroscopy
XPS	x-ray photoelectron spectroscopy

Acknowledgments

I would like to thank Drs. Elton Cairns and Frank McLarnon for their direction in this research project, especially for their patience in answering and reanswering questions ranging from electrochemistry to punctuation. In hindsight I must thank Dr. Cairns for persuading me to TA his electrochemical engineering course, from which I gained a more thorough understanding of the "basics."

I cannot go any further without offering thanks to ex-fellow-grad-student Jim Rudnicki for his friendship, insight, and invaluable help with anything to do with computers. He has, indeed, given help to many of us in the research group I am extremely lucky that he stuck around to do his postdoctoral work at LBL, at least until I finished writing this thing.

I would also like to thank those who have given me so much assistance with this project: Hubert Gasteiger for discussions on methanol oxidation; Dan Schwartz for his help with Raman; Lee Johnson for the initial work on making gas diffusion electrodes; and Kathy Striebel for saving me so much time by having already designed and made the test cell that was the centerpoint of my experiments

There are also those who have helped me maintain what mental stability I had during my time here through various distractions. For the mountain biking, hiking, golf, sailing, beers at Triple Rock, and maybe-too-

frequent coffee breaks, many thanks to Jeff, Paul, Gessie, Ken, Dan and Sue, Joel and Stacey.

I cannot thank my partner and wife, Sandra, enough for her loving support, patience, and strength in waiting this out with me. I know it was more than a little frustrating watching me take my own sweet time. Who knows how long this would have taken if she hadn't inspired and helped me without rushing me.

And thanks must go to my parents, Wilma and Bruce, for their long-distance support. They were happy, mad, indignant, and puzzled with me at all the right times; no small task.

This work was supported by the Assistant Secretary for Conservation and Renewable Energy, Office of Transportation Technologies, Electric/Hybrid Propulsion Division of the U.S. Department of Energy under contract No. DE-AC03-76SF00098.

Chapter 1. Introduction

Fuel Cells for Electric Vehicles 1
Methanol Fuel Cells.....3
Organization of Thesis.....4

Fuel Cells for Electric Vehicles

Fuel cells are electrochemical devices that directly convert available chemical energy into electricity. They can be distinguished from batteries in that batteries consume the active materials contained within the device, whereas fuel cells consume an externally-supplied oxidant and a fuel, usually hydrogen or an organic compound. As an **electrochemical storage device**, a battery can deliver only as much energy as that determined by the quantity of reactant stored in the electrodes. Conversely, the energy capacity of an **electrochemical conversion device**, such as a fuel cell, is determined by the quantity of fuel (and oxidant) available; so long as fuel is supplied, the fuel cell can continuously provide dc electricity. There are several excellent sources available that provide an overview of fuel cells and their operation [1-5]. The work covered in this thesis concerns experimental studies of the relationship between anode structure and performance in direct methanol fuel cells (DMFC) using aqueous carbonate electrolytes.

Specifically, we are interested in the anodic oxidation of vaporized methanol on Pt-Ru catalyst supported on high-surface-area carbon.

Several events have spurred renewed interest in electrochemical energy storage and conversion devices as power sources for many applications, particularly electric vehicles. Some key factors driving this interest include environmental issues, the desire to minimize dependency on petroleum-based fuel sources, dwindling natural resources, and higher theoretical efficiencies of fuel cells compared to internal combustion or other heat-engine systems. Most recently, several governmental and private organizations have placed increased emphasis on research and development of power sources for electric vehicles (EVs). This support has taken such forms as legislative actions[1] and joint government industry programs[2] in an effort to accelerate the introduction of viable electrochemical power systems to consumer vehicle markets.

Fuel cells have the potential to address the issues mentioned above: they have extremely low levels of emissions of toxic gases (including CO, SO_2, and NO_x) and reduced levels of CO_2 (a "greenhouse gas"); flexibility in the choice of fuels, reducing reliance on petroleum; and they have high theoretical efficiencies. In contrast to common energy conversion systems, which involve combustion and utilize the resultant heat energy, fuel cell efficiencies are not limited by the Carnot cycle and remain fairly constant

---

[1]Reference to the California Air Resources Board requirement that, by 1998, 2% of new automobiles sold in Los Angeles county must be zero-emissions.

[2]The United States Advanced Battery Consortium (USABC), a cooperative effort between government and private industry to develop a high-performance, rechargeable battery system for EVs, was established in 1991.

over a wide range of loads. Most research and development in EVs is driven by government funding or imposed legislation; presently, however, fuel cells can not compete with internal combustion engines in the open market.

Methanol Fuel Cells

Most methanol fuel cell systems under study for EV applications actually operate on hydrogen derived from reformed methanol. Ideally, the fuel cell would directly oxidize the methanol, eliminating the need for a reformer and its accompanying weight, bulk, and traditionally slow response characteristics. However, some major obstacles must be overcome before acceptable performance can be achieved with direct methanol fuel cells (DMFCs): methanol oxidation rates are several orders of magnitude below that of hydrogen on Pt catalyst, some oxidation products other than CO_2 and water are formed, especially in acidic electrolytes, and methanol dissolved in the electrolyte will diffuse to and react at the cathode.

There is a limited volume of work on methanol electrooxidation that has addressed these problems by the use of carbonate electrolytes [6-9]. Of particular interest is the work of Cairns and Bartosik [6], who investigated the direct oxidation of methanol using concentrated cesium and rubidium carbonate electrolytes . They found that the electrolyte remained invariant while generating reasonable power levels, and that the fuel was oxidized completely to CO_2 and H_2O. Their work is the basis for the research contained in this thesis, in which we investigate optimization of the gas diffusion electrode (GDE) structure with a bimetallic catalyst formed of Pt and Ru dispersed on high-surface-area carbon. The work done recently by Giner *et al.* [8] is quite similar to that by Cairns *et al.*, except that the

catalyst was Pt supported on high-surface-area carbon and the cell was operated at elevated pressures.

Organization of Thesis

Chapter 2 provides some background on prior research concerned with the direct oxidation of methanol using gas diffusion electrodes and aqueous electrolytes, both acidic and alkaline systems. The section covers the methanol oxidation reaction in various electrolytes, the surface reaction mechanisms that have been proposed for Pt catalysts, and research involving Pt-based co-catalysts.

Chapter 3 describes the experimental equipment and procedures used in developing and characterizing both the electrodes and the catalysts used in the electrodes. The catalysts, Pt or Pt-Ru supported on carbon, were formed into an electrode by mixing with a polytetrafluoroethylene (PTFE) suspension to form a slurry, which was then pressed onto wet-proofed graphite paper. The catalyst and support were characterized by Brunauer-Emmett-Teller (BET) nitrogen adsorption, Laser Raman Spectroscopy (LRS), and x-ray diffraction (XRD). The gas diffusion electrode was characterized by cyclic voltammetry, to indicate the wetted surface area of catalyst, and steady-state polarization, to measure performance. Additionally, the cell and electronic equipment used in the voltammetry and polarization experiments are described.

Chapter 4 details the experimental results for various electrode structures in the direct oxidation of methanol in aqueous carbonate electrolytes. The anode performance is shown as a function of temperature and of PTFE content in the reaction layer. Not much research has been

devoted to methanol fuel cells using carbonate electrolytes; some results are shown for comparison.

In chapter 5, some conclusions are drawn to suggest possible optimum electrode structures for the direct oxidation of methanol in aqueous carbonate electrolytes. In addition, some recommendations are made for future work, including examination of other catalyst compositions and the extension of this work to full cells, *i.e.*, a complete methanol/oxygen fuel cell.

Chapter 2. Background

Direct Oxidation of Methanol in Aqueous Electrolytes.....6
Gas Diffusion Electrodes 9
Methanol Oxidation on Platinum and Platinum-Based Co-catalysts 12
Studies on Platinum 12
Studies on Bimetallic Catalysts 15

Direct Oxidation of Methanol in Aqueous Electrolytes

Despite the favorable anode performance which has been realized using hydrogen as a fuel, the present technology concerning storage and transportation of molecular hydrogen precludes its use in fuel cells for EV applications[3]. Methanol offers several advantages over hydrogen as a fuel: it is much cheaper than hydrogen and is easily manufactured from coal or natural gas (thus, taking advantage of relatively abundant national resources), and, because it is liquid up to 65°C, it can be utilized in the fuel supply infrastructure presently used for gasoline.

Two distinct routes are being pursued in the use of methanol as a fuel. Much attention has been given to reformed methanol fuel cells. In this

[3]Approximately 98% of the weight in a hydrogen-filled container is the container itself. Also, hydrogen diffusion into the metal wall of the container may cause embrittlement and potentially catastrophic failure.

system, the methanol is converted in a reformer, which delivers a gas stream consisting of approximately 75% H_2 and 25 % CO_2, after water-gas-shifting to reduce CO content to ppb levels.

A more attractive alternative is to directly oxidize the methanol at the anode surface. The reaction mechanism and resultant products which accumulate at the anode are dependent on the electrolyte composition. In acidic electrolytes (as well as in proton conducting membranes), the overall reaction is rather straightforward. Hydrogen ions are generated at the anode surface by the following overall reaction

$$H_2O + CH_3OH \rightarrow CO_2 + 6H^+ + 6e^- \qquad [2\text{-}1]$$

The hydrogen ions then migrate across the electrolyte and are consumed at the cathode by reacting with oxygen, completing the electric circuit

$$\tfrac{3}{2}O_2 + 6H^+ + 6e^- \rightarrow 3H_2O \qquad [2\text{-}2]$$

Addition of these two half-cell reactions gives the resulting overall cell reaction for the methanol/oxygen system as follows

$$CH_3OH + \tfrac{3}{2}O_2 \rightarrow CO_2 + 2H_2O \qquad [2\text{-}3]$$

In alkaline systems, specifically those with electrolytes in which the principal conducting ion is the hydroxyl ion (OH^-), the reaction consumes the electrolyte in the main anode reaction as

$$CH_3OH + 8OH^- \rightarrow CO_3^{2-} + 6H_2O + 6e^- \qquad [2\text{-}4]$$

Besides the fact that only six Faradays of charge are produced while eight moles of hydroxyl ions are consumed, the electrolyte becomes contaminated by the carbonate ions and is therefore variant in composition. The buildup of

carbonate ions has several detrimental effects on fuel cell performance, including reduced oxygen solubility and electrolyte conductivity, increased electrolyte viscosity, and eventual precipitation of carbonate salts in the electrode pores [1]. There are also several other possible reactions at the anode that result in the production of undesirable ionic species, for example formate ions. At the cathode, the oxygen may react with water to form hydroxyl ions:

$$\tfrac{1}{2}O_2 + H_2O + 2e^- \rightarrow 2OH^- \qquad [2\text{-}5]$$

In the concentrated carbonate electrolyte system, the postulated reaction at the anode [6] involves the consumption of carbonate ions

$$CH_3OH + 3CO_3^{2-} \rightarrow 4CO_2 + 2H_2O + 6e^- \qquad [2\text{-}6]$$

followed by three of the carbon dioxide molecules being re-absorbed by the electrolyte to form bicarbonate ions

$$3CO_2 + 3H_2O + 3CO_3^{2-} \rightarrow 6HCO_3^- \qquad [2\text{-}7]$$

which then react with oxygen at the cathode according to the half reaction

$$\tfrac{3}{2}O_2 + 6HCO_3^- + 6e^- \rightarrow 6CO_3^{2-} + 3H_2O \qquad [2\text{-}8]$$

Addition of Equations 2-6, 2-7, and 2-8 gives the same overall reaction for the oxidation of methanol as given in Equation 2-3.

For direct methanol oxidation, the most appropriate method of delivery of methanol depends on the operating conditions of the system. If the cell operates at low temperatures (*i.e.*, lower than 65 °C , the boiling point of methanol) methanol must be supplied in liquid form to the electrolyte. In

such a case, because methanol would react directly at the cathode, the cell must contain some type of separator between the anolyte and catholyte that would allow charge-carrying species to pass but would prevent diffusion of the methanol. There are two major drawbacks to this proposal. First, experimental work shows that methanol readily transports across membranes commonly used in polymer electrolyte membrane fuel cells and chemically reacts at the cathode according to Equation 2-3. This problem, confirmed in recent mathematical models by Verbrugge [10] on perfluorinated membranes, suggest that membrane materials other than perfluorinated types should be investigated for viability in direct methanol fuel cells. Second, even if a membrane, which was selective to protons but not methanol, was developed, characteristically they all impose a significant resistance to the transport of ions and are, therefore, a source of ohmic loss.

As discussed in the next section, above 65 °C higher performance can be realized using vaporized methanol . It should be noted that, although a substantial amount of work has been done on surface studies, performance tests, and optimization of electrode structure for methanol oxidation with various electrocatalysts and electrolytes, the bulk of earlier research has been carried out with methanol dissolved in acidic electrolytes. There is, therefore, a considerable incentive for the study of oxidation of vaporized methanol in carbonate electrolytes.

Gas Diffusion Electrodes

As an alternative to mixing the methanol directly in the electrolyte, the fuel can be delivered in gaseous form to a gas diffusion electrode (GDE). Such an electrode is characterized by three distinct elements: a gas supply

layer; an electrocatalytic layer; and an electronically conductive pathway connecting the reaction surface with the external circuit. Some of the original work on gas diffusion electrodes is reported by Niedrach and Alford [11, *op. cit. loc.*], Cairns and others [6], and Kordesch *et al.* [12] provide a good description of their construction. Generally such electrodes are formed of a hydrophobic binder, such as PTFE, which forms a gas-permeable phase, and a mixture of PTFE and a high-surface-area powdered catalyst, forming an electrolyte-wetted network. In the electrodes of Niedrach and Cairns, the gas diffusion layer is a thin film of PTFE formed by spraying a dilute PTFE suspension onto a foil and slowly drying the film. The reaction layer is formed of a mixture of Pt-black and PTFE, which is then pressed against the PTFE film and heated to sinter the PTFE and bind the entire structure. These electrodes showed good performance on an area basis, however, the loadings were extremely high (at 30-40 mg Pt/cm^2), therefore performance on a mass-activity basis was inferior compared to present technology.

Recent work to prepare higher-performance electrodes has utilized an electrocatalyst, usually Pt or other noble metal, supported on high-surface-area carbon. Very high performance has been reported in acid electrolytes by Watanabe, Motoo and others [13-14151617], and in polymer electrolyte fuel cells by Gottesfeld *et al.*, at Los Alamos National Laboratory [18], and Srinivasan *et al.* [19]. Reported metal loadings have been reduced to 0.5 mg Pt/cm^2 or less, while maintaining equivalent performance on an area basis. It is important to note that the electrodes mentioned above were evaluated using oxygen reduction and/or hydrogen oxidation. Watanabe *et al.* did later apply their unique electrode structure to oxidation of methanol with supported Pt + Ru catalysts [20-2122]; however, the methanol was

either in the electrolyte [21] or supplied to the electrode by evaporation from a 2 M CH_3OH solution in contact with the gas diffusion layer [20].

In the porous gas electrode, the methanol diffuses through the electrolyte contained in the reaction layer pores to the catalyst surface where the reaction takes place. One must, therefore, consider several points in the construction of an active, optimized GDE: minimization of the diffusion resistance to the reactant and product gases in the gas diffusion layer; minimization of the diffusion resistance of the reactants and products in the electrolyte; maximization of active, available catalyst sites; attainment of high electronic conductivity in the electrode; and adequate chemical stability of all the electrode materials, including the catalyst and support (if any). Additionally, it is preferred that the three-phase (*i.e.*, electrolyte, catalyst, fuel/oxidant) region be stable to give more predictable behavior, *i.e.*, that the electrolyte "front" not shift with variations in operating conditions.

It should be reiterated that most work has been on hydrogen oxidation or oxygen reduction in acidic electrolytes. Some exceptions to this is the work by Watanabe on methanol in acids (mentioned above), and work by Cairns *et al.* for methanol in carbonates [6] and long-chain saturated hydrocarbons (up to ten carbons per molecule) in HF electrolytes [23, 24]. Again, there remains much work, which can be done on methanol oxidation with unique electrocatalyst and electrolyte combinations.

Methanol Oxidation on Platinum and Platinum-Based Co-catalysts

Studies on Platinum

A thermodynamic potential, representative of the energetics for the anodic oxidation of methanol according to the half-cell reaction given in Equation 2-1, can be calculated from the standard Gibbs free energies of the reactants and products, from which one finds a value of approximately 44 mV[4]. In practice, however, the open circuit potential for methanol on Pt is far anodic to the thermodynamic value, and in fact rests above 400 mV [25]. This large difference, or overpotential, has been attributed to a strongly adsorbed intermediate species formed on the surface of the Pt, which essentially poisons the reaction.

To appreciate the development of bimetallic catalysts, one must first understand the mechanism for methanol oxidation on Pt. Unfortunately, this is no simple matter. Although there is agreement on the general pathway for the methanol oxidation reaction, there remains substantial controversy regarding the actual nature of the poisoning intermediate, which is recognized as the limiting factor in the oxidation reaction rate. One of the most widely cited mechanisms for the electrooxidation of methanol in acidic electrolytes, proposed by Bagotzky *et al.* in 1977 [26, 27], involves the

---

[4]All potentials will be referenced to a Reversible Hydrogen Electrode (RHE) in the same electrolyte, at the same temperature, unless otherwise noted.

following reaction sequence:

$$CH_3OH \rightarrow \underset{xxx}{C}-OH + 3H^+ + 3e^- \qquad [2\text{-}9]$$

where the index *xxx* represents three valence bonds with the surface.

$$\underset{xxx}{C}-OH + OH_{ads} \rightarrow \underset{xx}{C}=O + H_2O \qquad [2\text{-}10]$$

$$\underset{xx}{C}=O + OH_{ads} \rightarrow \underset{x}{C}OOH \qquad [2\text{-}11]$$

$$Pt-COOH + Pt-OH \rightarrow CO_2 + H_2O \qquad [2\text{-}12]$$

Adsorbed radicals OH_{ads} are formed in acid solutions

$$H_2O \leftrightarrow OH_{ads} + H^+ + e^- \qquad [2\text{-}13]$$

and in alkaline solutions

$$OH^- \leftrightarrow OH_{ads} + e^- \qquad [2\text{-}14]$$

The methanol oxidation reaction, as described above, requires the concurrent adsorption of methanol and oxygen-containing species (*i.e.*, H_2O or OH-radicals). High initial currents are observed at potentials cathodic of 400 mV, but drop off rapidly (on the order of milliseconds) by four to five orders-of-magnitude as reported by McNicol *et al.* [28, 29]. These initial currents are attributable to the "stripping-off" of the first three, loosely held hydrogens (as summarized in equation 2-9). In spite of its high catalytic activity for the adsorption and dehydrogenation of methanol, Pt does not adsorb water at potentials below approximately 400 mV, thus leading to the high open circuit potential observed experimentally. One of the driving

forces in the research on co-catalysts is to find a second metal that is able to promote the formation OH at substantially lower potentials than Pt.

Bagotzky emphasized that the three hydrogen atoms are split off from the methanol in a three-step process, and that "COH is practically the only chemisorbed particle formed...." Later work by Willsau *et al.* [30, 31] corroborated this statement. Using an *in situ* mass spectroscopic technique (DEMS) to detect volatile and gaseous electrochemical products, they were able to record the results of the mass spectrometer in parallel with the charge passed in oxidizing adsorbed species to determine that the adsorbate was COH.

Despite advances in experimental methods for examining surface species, especially in the last decade, there remains substantial controversy as to the composition of the surface species. As recently as 1988, Parsons *et al.* [32] stated in a review of fuel cell research in the 1980s that "there is little doubt now that the poisoning intermediate has been identified unambiguously as CO and not COH as believed previously [by the same authors]." Parsons goes on to state that studies showing COH as the adsorbed species are subject to other interpretations, although he acknowledges that available surface areas and structures of the catalyst (*e.g.*, different crystal faces of Pt) result in varying coverage by poisoning species. Similarly, Leger and Lamy [33] note that *in situ* EMIRS studies led to the first "unambiguous proof of the presence of adsorbed CO on Pt electrodes during the adsorption of methanol."

Ironically, studies by Vielstich *et al.* published in 1988 [34] show COH as well as CO, the ratio of the two depending on the adsorption conditions, with the COH preferred at low coverage. Additionally, in the same year, Christensen *et al.* [35] using *in situ* IR spectroscopy identified COH as the

main adsorbed intermediate, but noted that at low potentials where the concentration of OH_{ads} is low, COH_{ads} may convert to CO_{ads} (as in Equation 2-10). The CO_{ads} species was assumed to be more difficult to oxidize than COH_{ads}, and therefore acts as the poison, and is "burnt off" only at more positive potentials.

Almost all spectroscopic studies of methanol oxidation on Pt have been done on smooth electrode surfaces in acidic media. The most effective *in situ* techniques (*e.g.*, SNIFTIRS) require mirror finishes and are not yet possible on porous carbon-based electrodes, although such studies would be of great interest. Work by Christensen *et al.* using SNIFTIRS [35] reveals that the CO_{ads} poison, which is detected on bulk Pt, does not form on small Pt particles supported on carbon, indicating a different poisoning mechanism. Although *ex situ* methods exist (*e.g.*, ECTDMS), which work well regardless of the electrode structure, for the identification of reaction intermediates, they are of limited value in detecting surface poisons.

Studies on Bimetallic Catalysts

Although it is appealing to think that, based on the theories of methanol oxidation on Pt discussed in the previous section, one could single-out Ru or any other second metal as an obvious choice for the second metal in a Pt-based bimetallic catalyst, it has been necessary to carry out extensive studies by trial-and-error. Various combinations of materials known to be electrocatalytically active have been examined, especially in the last two decades when methanol oxidation has gained such attention, and several good reviews exist [*e.g.*, references 32, 36].

Of the pure noble metals, Pt has the highest catalytic activity for the oxidation of methanol in acid solutions; however, studies have shown certain

combinations to have increased activity, especially Pt-Ru, Pt-Sn, and Pt-Re. Table 2-1 gives a listing of many of the papers that report on the performance of Pt with second metals for methanol oxidation. This list is not exhaustive, however, the preponderance of the results indicate Pt-Ru to be the most active electrocatalyst for methanol oxidation. Additionally, several research groups found performance optimized for a 50:50 (atomic ratio) mixture of Pt and Ru [22, 32, 42].

A substantial volume of work has been directed toward surface studies of Pt-Ru catalysts in an effort to understand the mechanism by which Ru increases catalytic activity for methanol oxidation. It should be emphasized that even now, as with determining the actual poisoning species on Pt, there remains controversy over the role that Ru and other additional species play in accelerating the reaction rate for methanol oxidation. Several mechanisms have been postulated including modification of the electronic nature of the surface[5], blocking of the poison formation reaction, and co-adsorption of oxygen-containing species which can then take part in the main oxidation reaction[6].

---

[5]Examples of this effect are given by Janssen *et al.* [45, 49], who explain the "ligand" effect of ad-atoms, and intraalloy electron transfer discussed by Goodenough *et al.* [42]

[6]Ticanelli *et al.* find a chemisorbed oxygen species on the Pt-Ru alloy at potentials as low as 0.25 V vs. RHE [69]; Watanabe *et al.* refer to the bifunctional theory of electrocatalysis with the Ru atoms adsorbing water at 350 mV vs. 750 mV on Pt.

Table 2-1. Performance studies for methanol oxidation on Pt-based, bi-metallic catalysts[7]

Subject	Year	Comments	Ref.
Review	81		36
Review	87	Buffered carbonate electrolytes	7
Review	87		37
Review	88		32
Review	88	Acidic and alkaline electrolytes	9
Review	90		33
Re	67		38
Ru	68	Pt-Ru on B_4C (CO-tolerance study)	39
Ru	72	Raney-type (XRD results)	25
Ru	75	H_2 fuel (CO-tolerance study)	40
Ru	84		21
Ru	86	Best if exposed to air at 250 °C	20
Ru	87	Optimum 50:50 a/o (XRD and XPS)	22
Ru	88		41
Ru	89	Optimum at 55:45 a/o	42
Ru	91	Supported on Vulcan	43
Sn	76	Ad-atom, alloy, co-electrodeposited	44
Sn	77	Ad-atom, alloy, co-electrodeposited	45
Sn	85	Ad-atoms on Pt-black	46
Sn	90	Single-crystal of Pt_3Sn	47, 48
Almost all	76	Best were Ru and Sn	49
Sn, Pb, Re, Ru	81	Ru best	50
Sn, Ge, As, Sb, Ru	86	Tested as ad-atoms, Ru best	51

[7]Listing of some representative studies on relative performance of platinum-based co-catalysts for the oxidation of methanol. Unless otherwise noted, the electrolyte used was acid.

Understanding the methanol oxidation mechanism on Pt-Ru is intimately related to determination of the catalyst surface structure, which is, in turn, a function of the bulk catalyst structure. A variety of catalyst structures have been studied including flat bulk alloys, high-surface-area bulk alloys (Raney type), finely-divided unsupported alloys (Adams type), and supported alloys (*e.g.*, on carbon, silica, or boron carbide). Of greatest interest, in relation to the present work, are supported Pt-Ru catalysts. X-ray Photoelectron Spectroscopy (XPS), valuable for characterization of many bimetallic systems, is less effective in this system due to interference of the signal from the carbon support (the C(1s) signal), which obscures the Ru signal (Ru(3d) lines). Hamnett and coworkers have combined ^{99}Ru Mössbauer studies on carbon-supported Pt-Ru [52] with XPS studies on unsupported Pt-Ru electrodes [41] at conditions for methanol oxidation, and have found strong evidence of an oxidized Ru species, specifically Ru(IV), possibly acting in a redox mode to accentuate the activity of the Pt. It is interesting to note that McNicol and Short [53] also find evidence of Ru (IV) in Ru Adams oxide catalyst using TPR. However, Janssen and Moolhuysen investigated Raney-type catalysts and, having found that the groups of catalysts exhibiting redox behavior at low potentials had lower activity for methanol oxidation than Ru [49], disputed the redox theory and promoted the concept of an electronic or "ligand" effect. Goodenough *et al.* [42] have combined XPS (particularly the Ru(3p) line, which is clear of the carbon-substrate signal), EXAFS, and ESR to support their assertion that synergistic catalytic effects result from an intraalloy electron transfer from Ru to Pt.

McNicol *et al.* have studied the influence of activation conditions on Pt-Ru performance by heat-treating both supported and unsupported, Raney-type alloys in different atmospheres (hydrogen, air, and oxygen) [54]. In their work they found the highest activity after treatment in oxygen (at temperatures above 300 °C)[8], attributing the increased activity to surface enrichment of Ru. However, recent UHV spectroscopic studies on smooth Pt-Ru alloys by Gasteiger *et al.*[55], in which both metals are meticulously maintained in their reduced state, show methanol activity that increases in direct proportion to the Pt content. Additionally, Gasteiger *et al.* found that, if the Pt-Ru alloy is exposed to an appreciable oxygen pressure at elevated temperatures (>300 °C), the Pt-Ru (oxidized) alloy activity exceeds that of pure Pt. Subsequent XPS studies of this alloy reveal an Ru oxide had been formed although the exact composition of the oxide has not yet been determined. These results would seem to lend another interpretation to the results of McNicol upon heating a Pt-Ru alloy in air, specifically, that the increased activity observed is due to the formation of an oxide; not an unlikely occurrence considering the conditions to which the alloy was exposed.

---

[8]This type of heat-treatment was later repeated by Watanabe *et al.* [20], who found an optimum treatment at 250 °C in air, but they merely reiterated the conclusions of McNicol.

Chapter 3. Experimental Procedures

Introduction....20
Electrode Fabrication....22
Gas Diffusion Layer....22
Catalyst....23
Pressing the Electrode....27
Cell Performance Studies....28
Electrolyte....28
Cell Configuration....29
Methanol Vaporization....36
Polarization Curves....37

Introduction

The primary motivation of this work was to optimize the macro-structure of a gas diffusion electrode for the oxidation of vaporized methanol on Pt-Ru in concentrated cesium carbonate (Cs_2CO_3) electrolyte. Anticipating the large number of variations in structure necessary to identify important relationships, we felt it would be more efficient to prepare these electrodes in-house. Since a need to vary catalyst content and composition was also anticipated, we decided to produce all the catalyst in our laboratory.

The gas diffusion electrodes are bi-layered, consisting of a hydrophobic gas diffusion layer and a semi-hydrophilic reaction layer pressed together. The gas diffusion layer acts as pathway for the reactant and product gases,

physical support for the reaction layer, and current collector. In determining the method of construction of the electrodes, we considered available equipment and experience as well as available technology. Although there are scores of methods cited in literature, the one selected was to vacuum-pull a reaction layer, in the form of a slurry, onto the gas diffusion layer. This bilayer electrode was then pressed, under heat, to bond the layers.

Catalysts were also prepared in-house by co-deposition of metal-chloride salts from their aqueous solutions onto high-surface-area graphite. The deposited metal salt was then reduced to its zero-valence state in a hot H_2/N_2 stream. The catalyst loading (in weight of metal per unit cross-sectional area of the electrode) was varied by controlling the total metal-content of the catalyst and the thickness of the reaction layer. Catalyst loading was nominally 0.5 mg/cm^2, but with material loss during manufacture, was actually ca. 0.4 ($\pm$ 0.05) mg/cm^2. These loadings are much lower than that reported by Cairns [6] and are comparable to state-of-the-art fuel cell technology. An excellent review of techniques for preparation and characterization of highly dispersed electrocatalysts prior to 1977 was presented by Kinoshita and Stonehart [56]. For more recent technology, many of the reports on performance of catalysts for methanol oxidation describe methods for preparing the catalysts.

The catalyst and electrodes were evaluated several ways to characterize their physical and chemical structure. The surface area of the graphitized carbon support in the reaction layer was determined using standard BET tests, and the extent of graphitization determined with Laser Raman Spectroscopy. For Pt-Ru on graphite, x-ray diffraction was used to determine the state of the two metals, *i.e.*, simply co-deposited or alloyed. After the electrodes were constructed, cyclic voltammetry was used to

determine the surface characteristics of the catalyst such as the number of accessible active sites. The final measure was to determine the overall electrode performance by means of polarization experiments of methanol oxidation. The majority of the polarization curves were performed on Pt-Ru in concentrated cesium carbonate; however, some measurements were made for hydrogen oxidation in 1 M H_2SO_4 for comparison to results published by others.

Electrode Fabrication

As mentioned in the previous section the gas diffusion electrodes were bi-layered, and were made by pressing a gas diffusion layer and reaction layer together under heat. Details for the manufacture of the gas diffusion electrode are contained in Appendix B.

Gas Diffusion Layer

The gas diffusion layer was made from a polyacrylonitrile-based graphite paper TGP-120H (Toray Co., Japan) with the properties listed in Table 3-1. The graphite paper was soaked in a diluted PTFE suspension for several minutes; the concentration of the suspension and the soak time were adjusted to end up with a gas diffusion layer with a PTFE content between 45 and 55 % by weight (w/o).

Table 3-1. Physical Properties: TGP-120H Graphite Paper (Technical Data Sheet, Toray Co., Japan)

Bulk density [g/cm^3]	0.49
Electrical resistivity, through plane [Ω-cm]	0.07
Electrical resistivity, in plane [Ω-cm]	0.005
Flexural strength (est. from thicker samples) [kg/cm^2]	ca. 260
Gas permeability [mmaq/mm]	32
Porosity [%]	73
Thermal conductivity [cal/cm-sec °C]	6×10^{-3}
Thickness [mm]	0.35

Catalyst

As mentioned earlier, the catalyst was made in-house to give greater control and flexibility in the composition. The catalyst was Pt or Pt-Ru finely dispersed on graphitized carbon[9]. The carbon support was Vulcan XC-72R (Cabot), which has a reported surface area of ca. 250 m^2/g. This material was graphitized by heat-treatment at 2700 °C for one hour in an inert atmosphere (Fiber Materials, Inc.). BET tests on the graphitized Vulcan showed the surface area had been reduced to 72 m^2/g. The procedure followed in preparing the supported catalyst is shown in Figure 3-1. A "raw catalyst" was made first by soaking the carbon in a solution of the chloride salts of Pt ($H_2PtCl_6 \cdot 6H_2O$, Strem Chemicals, Inc., MA) and Ru ($RuCl_3 \cdot 3H_2O$, Strem

[9]Several batches of catalyst, and consequently several electrodes, were made with non-graphitized carbon to determine its effect on performance.

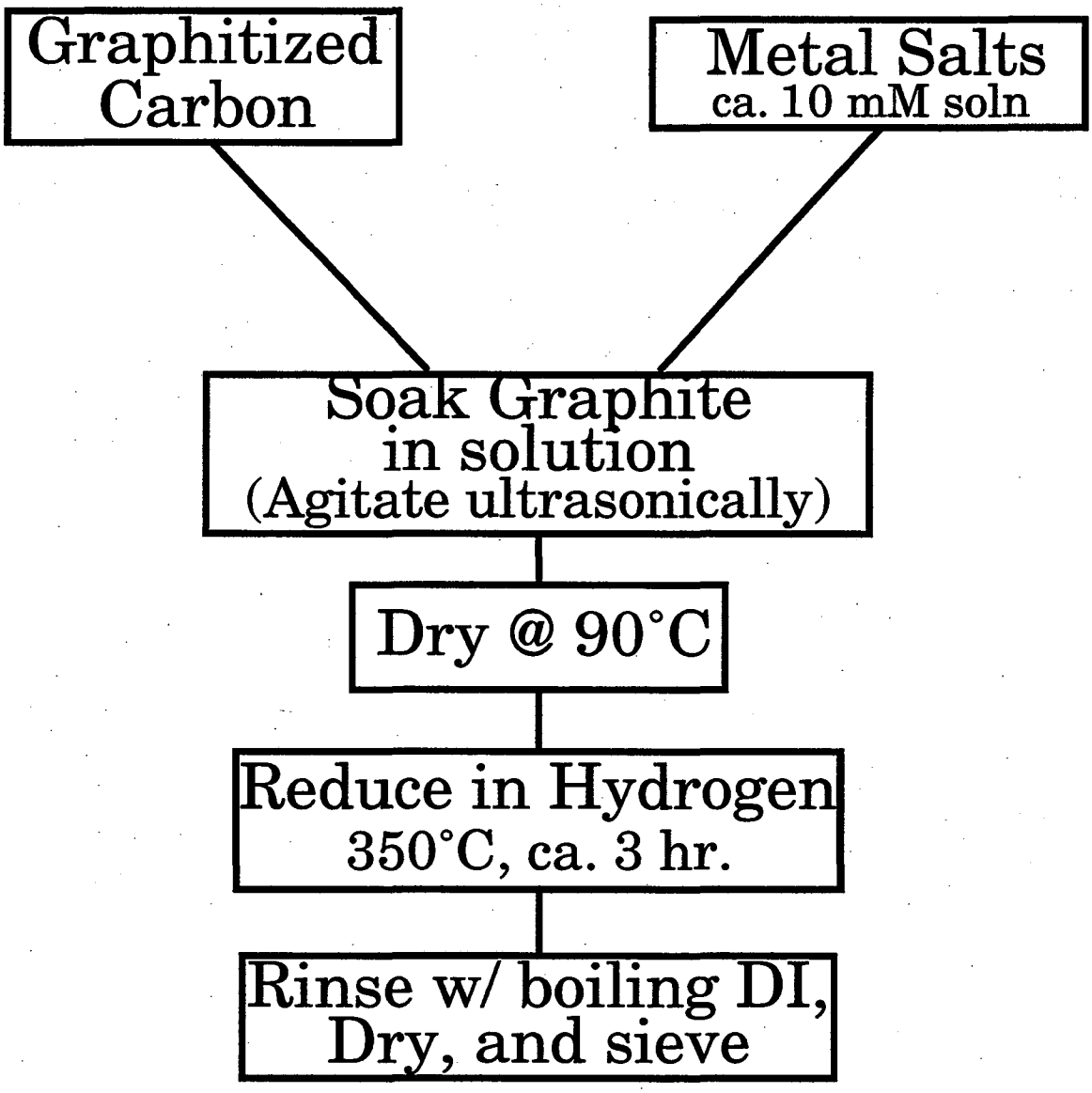

Figure 3-1. Procedure for making Pt and Pt-Ru supported on high-surface-area carbon.

Chemicals, Inc., MA) in equimolar volumes to give a final atomic ratio of 1:1 Pt:Ru. This solution was mixed with an ultrasonic horn (Model V-50, Vibracell Co.), making a thick slurry, and dried at 90 °C. The raw catalyst was reduced under flowing hydrogen and nitrogen in a quartz tube heated in a tube furnace. The reduced catalyst was then washed with copious amounts of boiling DI water to remove any trace amounts of chloride ions.

Laser Raman Spectroscopy (LRS) was used to examine the structure of the carbon catalyst support to determine its extent of graphitization. The Laser Raman Spectroscopy system (previously set up for studies of oxidation films on copper [57]) used an argon ion laser (tuned to 488 nm) as the excitation source, and a photo diode array detector. Details of the LRS instrumentation are given elsewhere [58]. Two lines appear in the Raman spectra of carbon, at 1355 cm^{-1} and 1575 cm^{-1}. The width and intensity of these lines, and the ratio of their intensities $R = I_{1355}/I_{1575}$, vary predictably with the extent to which the carbon is graphitized. As the carbon becomes more graphitized, the ratio R increases [59]. Tuinstra and Koenig [60] have equated this ratio with the "amount of crystal boundary" in the sample, which in turn is inversely related to the average crystal diameter (see Figure 3-2). The Raman spectra of the VG, as collected in this work, indicate a high degree of graphitization, with an average crystallite size (L_a) of 11 nm (see Figure 3-3)[10]. Included in Figure 3-3 is the Raman spectra for graphitized Sterling-R (Cabot), with the same heat-treatment, to show the different crystallite sizes, *i.e.*, 17 nm for the Sterling-R.

---

[10]The heating effect as repored by Ager *et al.* [61] was taken into account by extrapolating to zero laser power.

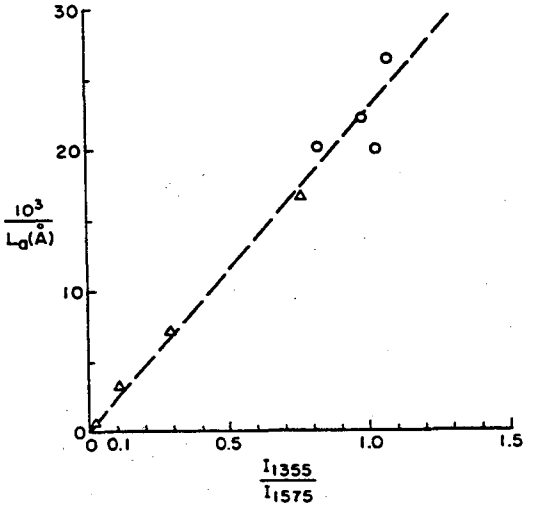

Figure 3-2. Linear relationship between the ratio of the Raman lines for carbon, R at 1355 cm^{-1} and 1575 cm^{-1}, and the crystallite size, L_a.

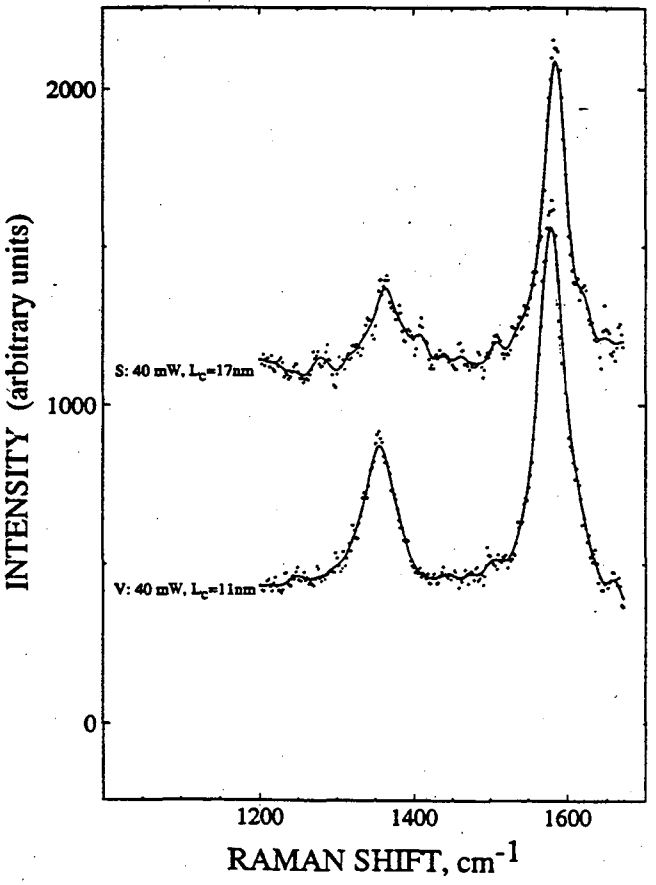

Figure 3-3. Raman spectrum of graphitized Vulcan XC-72R, used as catalyst support, with calculated crystallite size, L_a, of 11 nm.

Pressing the Electrode

The catalyst was mixed with a PTFE suspension (TFE-30, DuPont) diluted one part PTFE in nine parts water (by volume), and agitated with the Vibracell to form a slurry. This slurry was pulled onto the gas diffusion layer, using a vacuum table, to form the bi-layer assembly. The entire assembly was pressed several times at room temperature on a hydraulic press (Carver) with absorbent materials at pressures progressing up to 100 kg/cm^2. The first few pressing steps, while the reaction layer material was still wet, proved to be critical for several reasons. First, it was necessary to prevent any sticking to the absorbent materials, yet facilitate the transport of water away from the electrode surface. Second, any physical features in the absorbent materials were pressed into the electrode surface. This necessitated a material which would impart a very smooth surface and be easily removed after drying, with little or no adhesion to or delamination of the reaction layer. The final material selected and used was a micro-porous polypropylene film ca. 40 mm thick (Celgard, Celanese Co.).

This partially dried assembly was completely dried in an oven at 90 °C for several hours. The electrode was then sealed in an aluminum foil envelope, which was purged with nitrogen, and pressed at 340 °C for fifteen minutes on the hydraulic press at 100 kg/cm^2 to sinter the PTFE and form the network of hydrophilic and hydrophobic pores. Circular test electrodes of 2 to 3 cm^2 were cut from the 20 cm^2 (4 cm by 5 cm) electrode and weighed and measured to determine the actual catalyst loading.

Cell Performance Studies

Electrolyte

Polarization tests and cyclic voltammetry were performed in sulfuric acid and cesium carbonate electrolytes. All electrolytes were made by diluting stock reagents, used as received, to the proper concentration with water purified to a resistivity of at least 16 MW using a Millipore filtration system. All electrolyte solutions were further purified by electrolyzing with Pt screens overnight at low currents (*i.e.*, on the order of 1 mA). Sulfuric acid was prepared by diluting the appropriate weight of 98 % H_2SO_4 ("Baker Analyzed", Baker) with the Millipore water to 1 molar in a volumetric flask.

The concentrated cesium carbonate electrolyte was made by weighing out proper amount of 99.99 % pure solids (Johnson Matthey Electronics) and dissolving in 16 MW water in a fluorinated ethylenepropylene (FEP) transfer container. To operate experiments at elevated temperatures of 100 to 130 °C, cesium carbonate solutions were required with boiling points of 120 and 140 °C. As previously determined by Cairns [62], these boiling points correspond to solutions with concentrations of approximately 72 and 82 w/o, and freezing points of approximately 22 and 80 °C. Because of the elevated melting points, concentrated cesium carbonate solutions were prepared by pouring the appropriate volume of water into the transfer container, adding the weighed cesium carbonate powder, closing the container (to prevent evaporation), and mixing on a heated stir-plate until dissolved. During experiments, excess cesium carbonate was kept in an oven at 90 °C in the securely closed transfer container.

Cell Configuration

Tests were conducted using a half-cell arrangement. The cell was designed and used in previous research on oxygen reduction by Striebel *et al.* [63-65]. Due to the corrosive nature of the electrolyte, and the need to maintain a very high level of purity, all parts of the cell in contact with the electrolyte were constructed of either PTFE or Pt. As can be seen in the cell cross-section in Figure 3-4, the working electrode was positioned horizontally, sandwiched with a Pt mesh current collector between two PTFE plates with circular openings of 1 cm^2 above and below to permit contact with the electrolyte and the fuel in the gas phase, respectively. A photograph of the cell parts is shown in Figure 3-5. When operating at higher temperatures (*i.e.*, above 110 °C), the PTFE plates had a tendency to deform slightly under compression; this occasionally resulted in a compromised seal. To prevent this, an arrangement of FEP gaskets was used around the working electrode, as shown in the exploded detail in Figure 3-6. The gaskets, (a) in the figure, fit snugly around the raised inserts in the bottom and middle plates. Additionally, the Pt-mesh current collector was fitted with two FEP gaskets (melted on), which had inner diameters slightly smaller than the working electrode and outer diameters equal to the inserts in the plates.

The bubbling hydrogen reference electrode (RHE) was contained in a separate compartment that was threaded and screwed into the top plate of the cell. The connection to the main electrolyte chamber was made through a Luggin capillary, the tip of which could be positioned very accurately by turning the RHE compartment. The tip was maintained as close as possible to the surface of the working electrode without interfering with the current

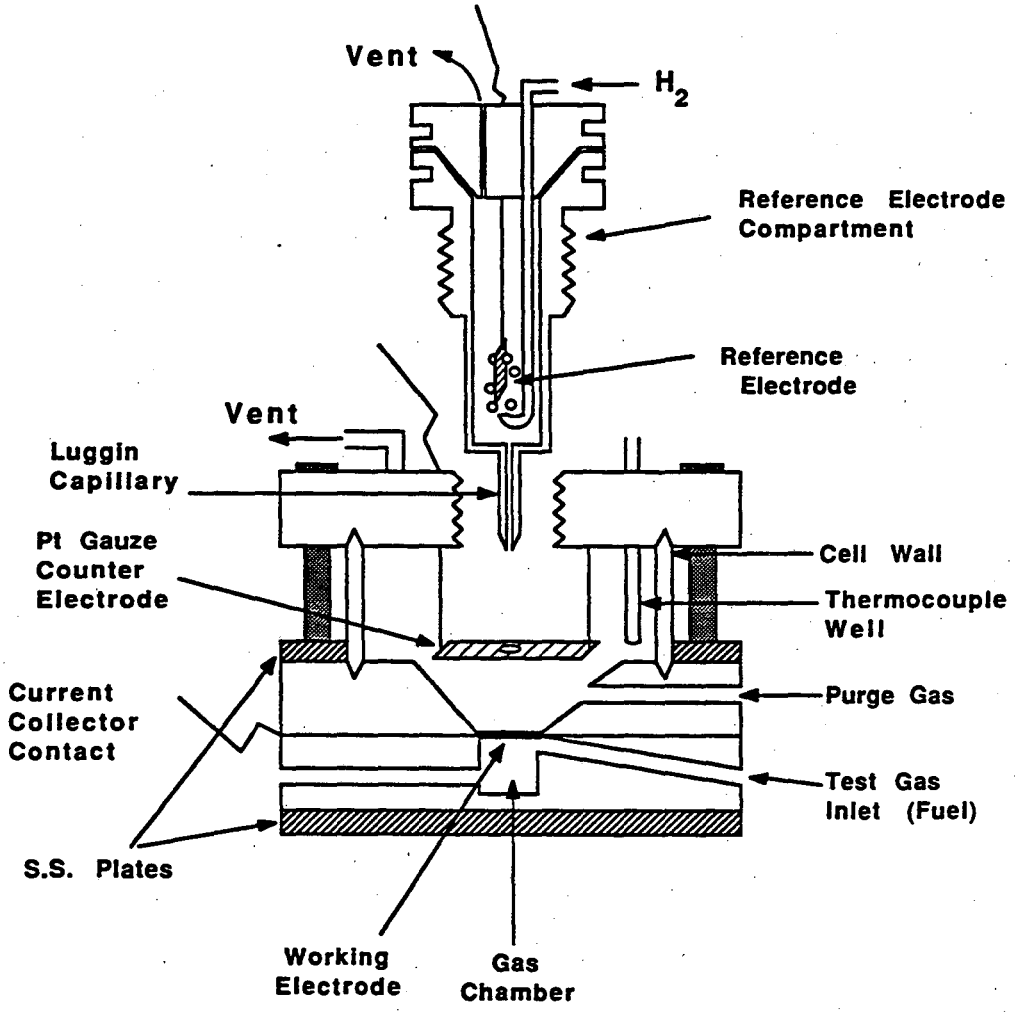

Figure 3-4. PTFE half-cell used in polarization and cyclic voltammetry experiments.

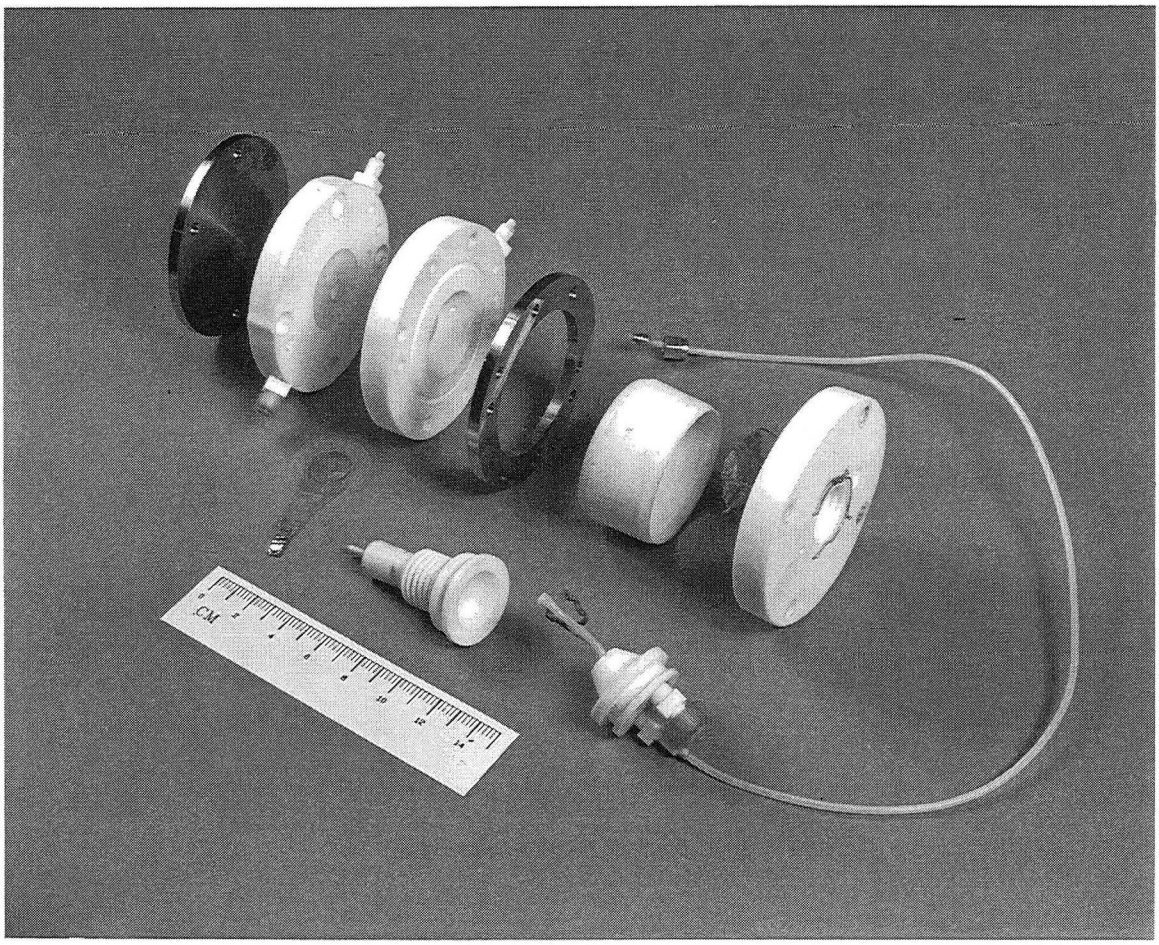

Figure 3-5. Photograph of cell parts.

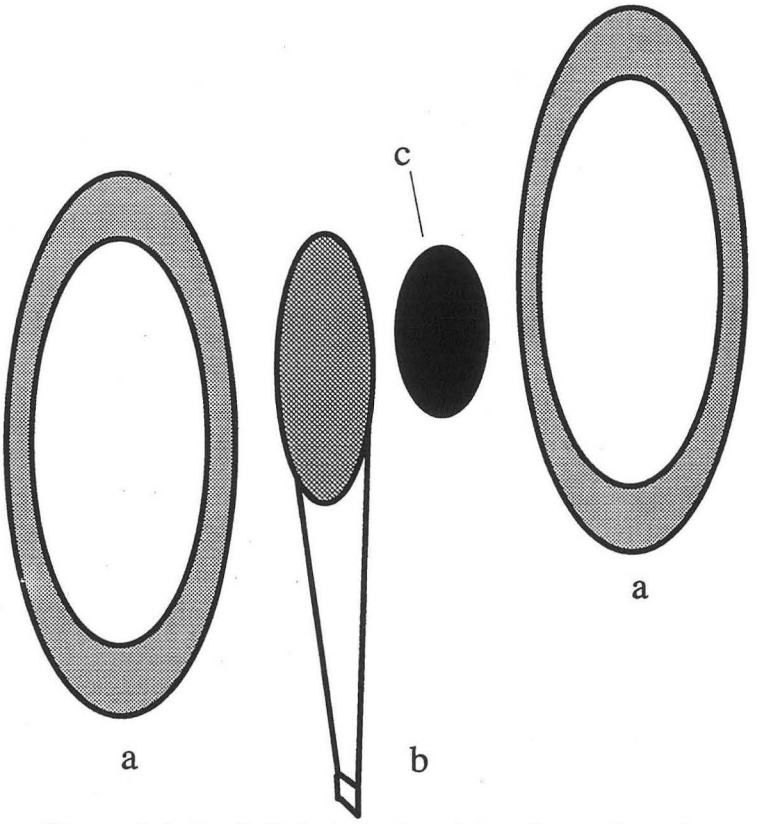

Figure 3-6. Exploded view of working electrode and gasket arrangement. a) FEP gasket (cut from 5 mil film); b) Pt mesh current collector; c) working gas diffusion electrode.

lines. The initial position was determined by screwing in the RHE compartment until the tip contacted the working electrode surface and then backing out the compartment approximately one quarter turn (ca. 1 mm of linear travel); this position was reproduced in subsequent experiments by using a shim of the appropriate thickness between the lip of the RHE compartment and the top plate. A fine Pt wire was placed in the Luggin capillary to ensure complete wetting by the electrolyte and maintain a conductive path. The tip of the Luggin passed through a hole in the counter electrode, a large-area Pt mesh.

The main body of the cell was equipped with an inlet for purge gas (through the middle plate), an outlet for the purge gas (through the top plate), and an opening that was used for either a thermocouple well or an inlet for an inert gas (through the top plate). The purge gases (N_2) were humidified by passing through water bubblers, which were contained in a temperature-controlled aluminum block, adjusted to maintain a water vapor pressure equivalent to that of the electrolyte. The bottom plate of the cell was equipped with passages for either the gaseous fuel or a purge gas. The passage opened as closely as possible to the back side of the working electrode to ensure intimate contact between fresh fuel and the gas diffusion layer. The outlet streams for the purge gas, the bubbling hydrogen stream, and the fuel gas were passed through gas traps. In the case of the purge gas and the hydrogen stream, the back pressure on the outlet tubes was maintained at a constant value by positioning the end of the tube in a water bath, to keep a steady electrolyte level in the reference electrode compartment.

The entire cell was contained in a thermostatically controlled oven (Model SK 3105, Associated Testing Laboratories, Wayne, NJ), arranged as

shown in Figure 3-7. Temperature could be controlled to within 1 °C of set point. Previous attempts to heat the cell by wrapping with heating tape were unsuccessful. The heating tape frequently caused hot spots (and occasionally failure of the tape itself or other PTFE components), and it was questionable as to whether the reference electrode chamber, which protrudes from the top plate, was at the same temperature as the rest of the cell. The oven had several openings in one wall, through which electrical leads, gas tubing, and the fuel feed passed.

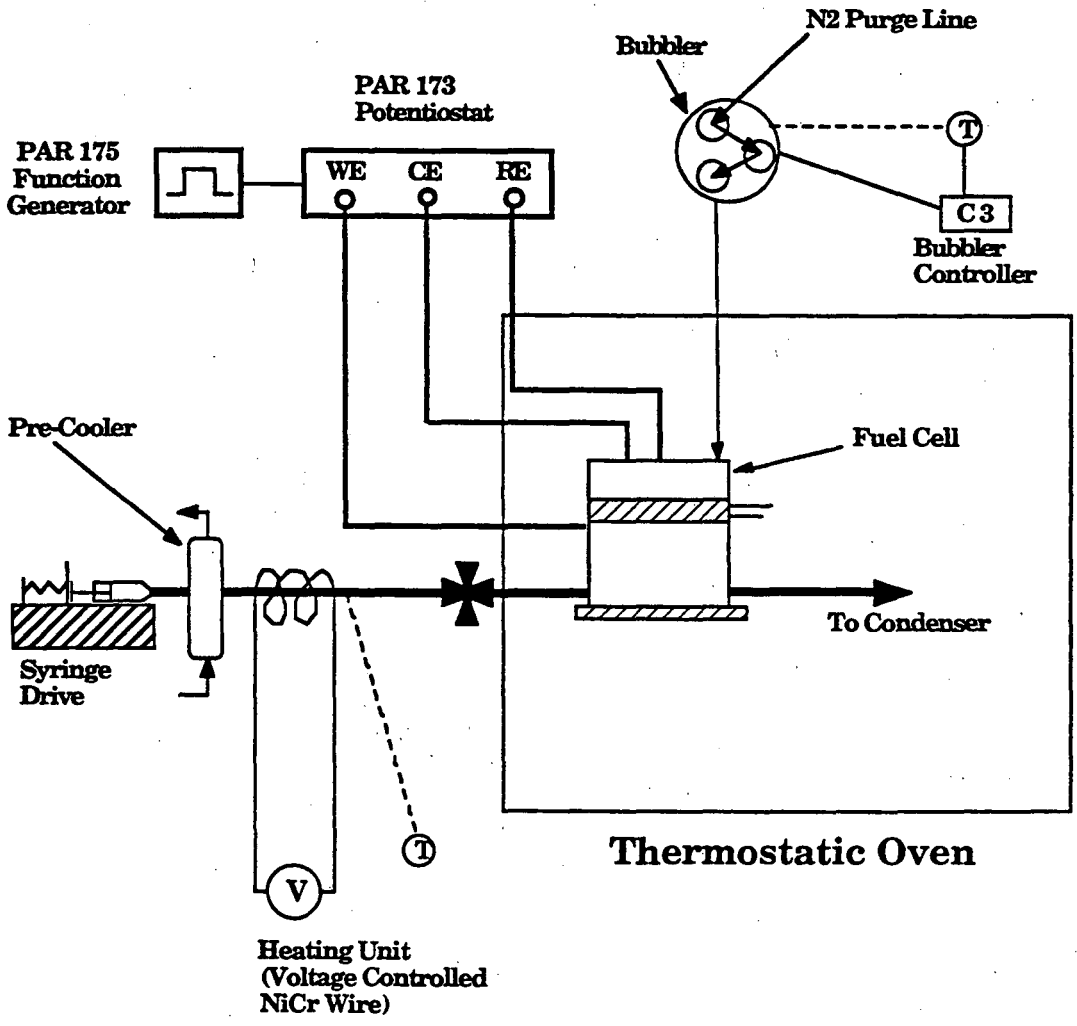

Figure 3-7. Diagrammatic arrangement of experimental setup.

Methanol Vaporization

To ensure accurate performance characterization, the methanol must be delivered in gaseous form, in a well-behaved manner. The method selected by the authors was based on that used by Cairns *et al.* [6], using pure methanol. It should be noted that most fuel cell tests found in the literature use a fuel stream that is not pure methanol; usually it is delivered by a carrier gas (such as nitrogen) and is frequently mixed with water. In this project, it was felt that a pure methanol fuel stream most closely represented EV system requirements, where additional weight from carrying nitrogen and/or water would be detrimental. Any water required in the anode reaction (see Equation 2-6, page 8) will be supplied from the electrolyte (formed at the cathode, see Equation 2-8, page 8).

The intention was to develop a system that delivered a pure methanol stream at a rate equivalent to approximately 50% fuel utilization. For a 1 cm^2 electrode at 1 A/cm^2 (much higher than attainable), this equals 8.386 µl/min of liquid methanol. Assuming vaporized methanol will act as an ideal gas, this corresponds to 5.266×10^3 µl/min of gaseous methanol at 65 °C delivered to the back side of the WE. This extremely low liquid-flow rate makes accurate delivery of the methanol difficult. However, the combination of a highly accurate syringe drive with an air-tight syringe makes these low flow rates manageable. The syringe drive, a Harvard Apparatus, Model 22, used in conjunction with a 1000 µl syringe (1000-Series Gastight, Hamilton-Microliter), allows accurate delivery rates from 0.049 µl/hr to 805 µl /min.

The methanol was delivered from the syringe to the cell through a stainless steel hypodermic needle, the end of which had been cut off. The needle was contained in a ceramic tube and secured with thermally

conductive epoxy (Omega). The ceramic tube was tightly wrapped with nichrome wire, which served as a heating element, and the entire assembly was encased with teflon shrink-wrap tubing. The ceramic tube had two passageways, with a thermocouple inserted halfway down the passageway not occupied by the needle.

Polarization Curves

Steady-state polarization data were the primary means of determining the performance of the electrodes. All measurements were made using a PAR Model 173 Potentiostat/Galvanostat in conjunction with an EG&G PAR Model 175 Programmable Controller and an EG&G PAR Model 376 Logarithmic Current Converter. Slow-sweep potentionstatic experiments were recorded on a Linseis Model LY18100 X-Y Recorder. Galvanostatically-controlled experiments were either recorded on the x-y recorder, or recorded by hand from a digital voltmeter connected to the Model 173 voltage output.

Polarization experiments followed a well-defined series of steps to maintain a consistent basis of comparison. The reaction layers of the test electrodes were extremely difficult to wet in the 1 M H_2SO_4, as well as the concentrated cesium carbonate; even prolonged soaking in the electrolyte (*i.e.*, over several days) gave only minimal, spotty wetting of the surface. A non-aggressive method was devised that gave thorough, reproducible wetting without flooding the reaction or gas diffusion layer. The reaction layer surface of the test electrode was first lightly pressed onto a lintless cloth (Texwipe) that had been dampened with methanol, then it was rinsed with DI water, and placed face-down into a beaker of 1 M H_2SO_4 for several hours.

Following the initial wetting procedures , the electrode was placed in the cell, which was then filled with 1 M H_2SO_4. The electrolyte was purged for several hours with pre-humidified nitrogen to remove dissolved oxygen, as was the backside of the working electrode. At this point, cyclic voltammograms were recorded to check for impurities, determine the extent of catalyst wetting, and characterize the catalyst surface. Most measurements were performed in the range of 0 to 1000 mV to avoid any possible complications from changing the structure of the catalyst surface (Ru is known to form oxides which are electrochemically irreducible, when taken to anodic potentials above about 1200 mV). The CVs were followed by a polarization test at 20 °C, using hydrogen as fuel, to develop a basis for comparison with results published by others.

The electrolyte was then changed to 72 wt% Cs_2CO_3, the temperature raised to approximately 50 °C, and the cell again characterized by cyclic voltammetry. The cell was then taken to 100 °C, cyclic voltammograms recorded, and polarization tests performed, this time with vaporized methanol. The CVs and polarization experiments were then repeated at 110, 120, and 130 °C. The electrolyte was again changed to 82 wt% Cs_2CO_3 while the cell was held at 100 °C[11] and the cyclic voltammograms and methanol polarization curves collected at 100, 110, 120, 130, and in a few cases 140 °C.

During methanol (or hydrogen) polarization in carbonate electrolyte, there was a build-up of bicarbonate ions (see Equations 2-6 and 2-7), especially in the anode pores. Because of the relatively large electrolyte volume (approximately 60 ml) and the lack of a cell-balancing reaction at the

---

[11]The melting point of 82 wt% Cs_2CO_3 is approximately 85 °C, therefore it was necessary to keep the cell above 100 °C to prevent solidification of the electrolyte.

cathode to regenerate carbonate ions (where, for example, the bicarbonate ions react with oxygen), a pH gradient steadily builds near the anode. To get a basis for comparison between different electrode runs, and in fact between different current-potential points for a single electrode, corrective adjustments were made to the potential to compensated for any local pH variations. At the onset of a polarization experiment, the open-circuit of the working electrode was recorded with hydrogen on the gas diffusion side. This offset value (if any) was then subtracted from each subsequent measurement to adjust for any initial pH gradient. The fuel was then switched to methanol, and the open circuit value recorded. Additionally, at each current-potential point, the current was interrupted and the open-circuit potential recorded. The final, adjusted potential for each current point was taken as

$$E^{x}_{adj} = E^{x}_{meas} - (E^{x}_{oc} - E^{o}_{oc} - E^{H_2}_{oc}) \qquad [3\text{-}1]$$

IR correction measurements were made by the current-interrupt method using a Nicolet Model 206 Digital Oscilloscope. The potential drop that was attributable to a purely ohmic resistance was that measured in approximately the first 100 ns following interruption of the current after a steady state value was reached.

Chapter 4. Results and Discussion

Characterization of catalyst 40
X-ray Diffraction 40
Cyclic Voltammetry 44
IR-Drop 52
Methanol Oxidation on Platinum/Ruthenium 54
Effect of Catalyst Composition 54
Effect of Temperature on Performance 58
Effect of Teflon Content on Performance 61

Characterization of catalyst

X-ray Diffraction

The normal crystal structure of pure Pt is face-centered cubic (fcc), while that of Ru is hexagonal close-packed (hcp). At atom fractions of Ru up to approximately 70 a/o, Pt and Ru form a solid solution, in which Pt atoms are replaced by Ru atoms on the lattice points of the fcc structure. Above approximately 70 a/o Ru, another solid solution phase is formed in which the Ru atoms are replaced by Pt atoms in an hcp structure. Using X-ray diffraction (XRD), one can determine the composition of the alloy by measuring the deformation of the crystal lattice. As seen in Figure 4-1, the lattice constant has been correlated to the atomic percent of Ru in Pt by Binder *et al.* [25]. The penetration of the x-rays is deep enough that XRD is a

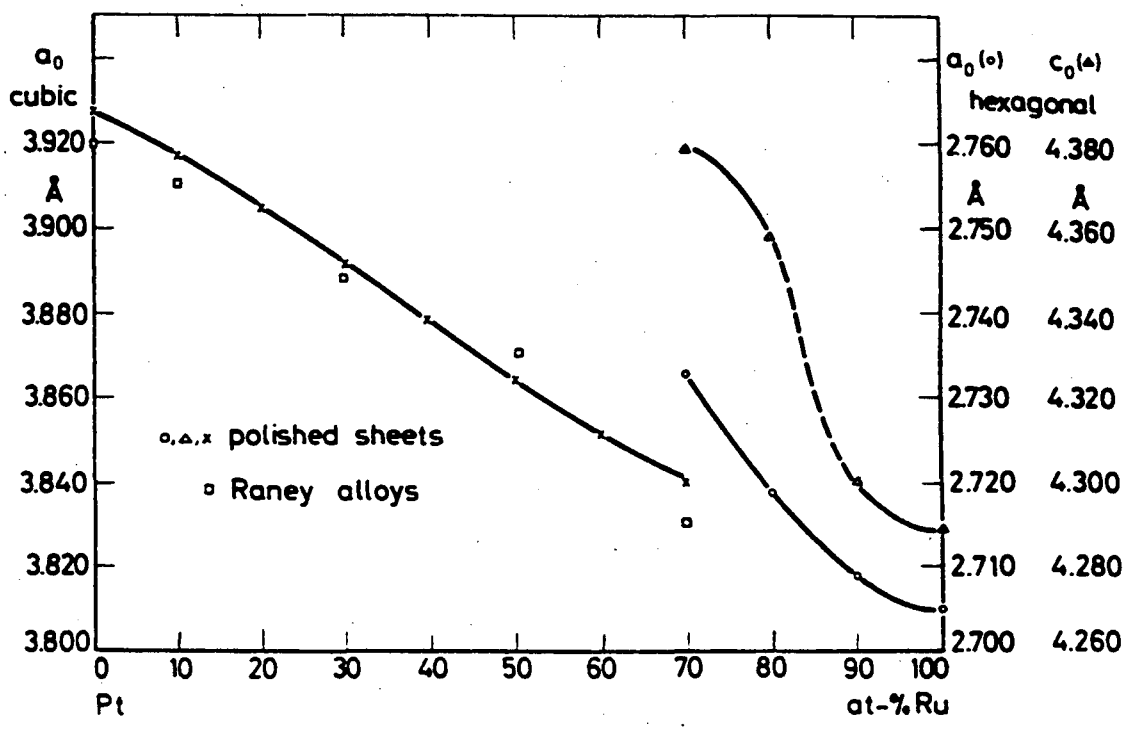

Figure 4-1. Lattice constants of Pt-Ru alloys as a function of alloy composition (by H. Binder *et al.* 25).

essentially a bulk method, and reveals information on the bulk structure of the catalyst and, in this case, of the support [66]. The structural work was performed on a Siemens Diffractometer (Model D500) using the Cu-K_{a1} radiation. Our results indicate a high percentage of pure Pt with a small amount of a Ru-rich alloy, although quantitative results are difficult to obtain. As seen in Figure 4-2 , there is essentially no shift in the Pt (100) peak, indicating that the Pt present is not in the alloy phase. Figure 4-3 shows the Ru (100) line; the offset from the pure-Ru reference line indicates a Ru-rich alloy with Pt. Neither spectrum reveals the presence of RuO_2. This not surprising due to the strongly reducing environment to which the catalyst was exposed during the manufacturing process. However, the environment while fabricating the electrodes is certainly oxidizing, despite efforts to provide a neutral atmosphere during sintering, and may alter the surface structure and composition of the catalyst.

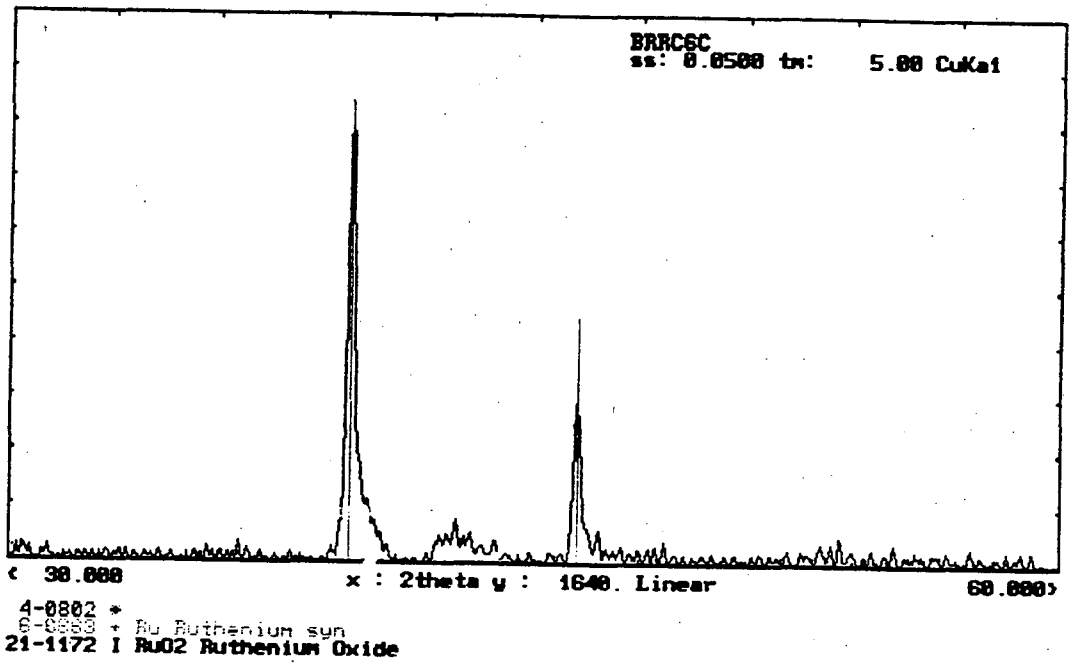

Figure 4-2. X-ray diffractogram of Pt-Ru (50:50) supported on graphitized carbon showing the Pt line.

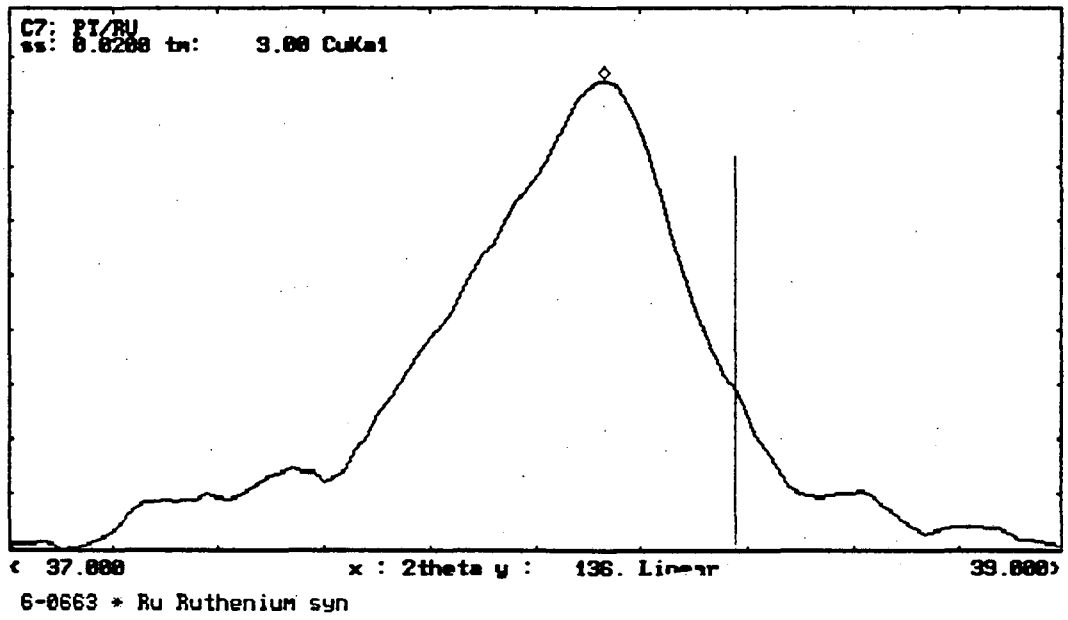

Figure 4-3. X-ray diffractogram of Pt-Ru (50:50) supported on graphitized carbon showing the Ru line.

Cyclic Voltammetry

Before going into detail concerning the cyclic voltammetry results, it is important to note that the acquisition of repeatable voltammograms was difficult at best. Even between electrodes with the same properties (*i.e.*, catalyst, teflon content, etc.) at the same conditions (sweep rate, temperature, electrolyte composition) there were difficulties reproducing certain features. In fact, examples of cyclic voltammetry in the literature vary significantly from author to author and make interpretation of features difficult at times. These problems, common with non-supported Pt-Ru, are exacerbated when the catalyst is supported on, for example, high-surface-area carbon.

The main purpose of the voltammetry in this work was to indicate, qualitatively, the composition and surface area of the wetted catalyst. The surface area of Pt is normally determined electrochemically by measuring the charge attributable to the removal of a monolayer of adsorbed hydrogen during an anodic voltammetric sweep, *i.e.*, from approximately 0 to 250 mV. It is well-recognized, however, that the presence of Ru complicates this type of measurement [25, 40, 67]. This is mainly caused by the early onset of oxide formation on Ru (relative to that of Pt) before the "double-layer" region, which starts at approximately 350 mV, complicating any clear-cut determination of the hydrogen desorption region. Ross *et al.* also encountered problems with electrochemical determination of Pt-Ru surfaces as well as with CO-chemisorption techniques, and ended up relying on a combination of X-Ray diffraction line broadening and electron microscopy [40]. However, an approximate value of the catalyst surface area can be determined if the double layer capacity is estimated and then subtracted from the hydrogen desorption region as explained by Binder *et al.* [25].

Cyclic voltammetry in this work had features similar to that in literature. Compared to Pt, Pt-Ru cyclic voltammetry shows loss of detail in the hydrogen adsorption/desorption region, much higher currents in the double-layer region, and large variation in features with changes in sweep rates, Pt-Ru composition, and treatment of the catalyst (*e.g.*, heat-treating in different atmospheres). Figure 4-4 shows several examples of cyclic voltammetry on supported and unsupported Pt-Ru-catalyst electrodes. The work by Binder *et al.* reveals the sensitivity of the catalyst response to structure and composition during cyclic voltammetry [25]. They have shown the contrast between polished-sheet alloy, Figure 4-4, curve (a), which shows strong Pt-like behavior, and a high-surface-area Raney alloy, curve (b), which is almost featureless (ironically, a feature of Ru voltammetry). The work of Kinoshita and Ross on Pt-Ru alloy supported on graphitized carbon [68], curve (c), shows more features, possibly a result of the higher potentials to which the electrode is cycled, the highly dispersed nature of their catalyst, and the influence of the carbon support on the catalyst. The i-V curve of this work, curve (d), is most similar to that of Kinoshita *et al.* both in the features and in the parameters of the cyclic voltammetry and the catalyst. It is of interest to note that although XRD experiments in this work indicated a predominance of Pt, the cyclic voltammetry clearly indicates the presence of Ru. The two methods of characterizing the catalyst are complementary: XRD reveals bulk properties of the catalyst due to the penetration of the x-rays, while cyclic voltammetry is useful for characterizing the surface composition and properties of the catalyst. The differences in the two results may be indicative of significant surface-enrichment by Ru in the alloy.

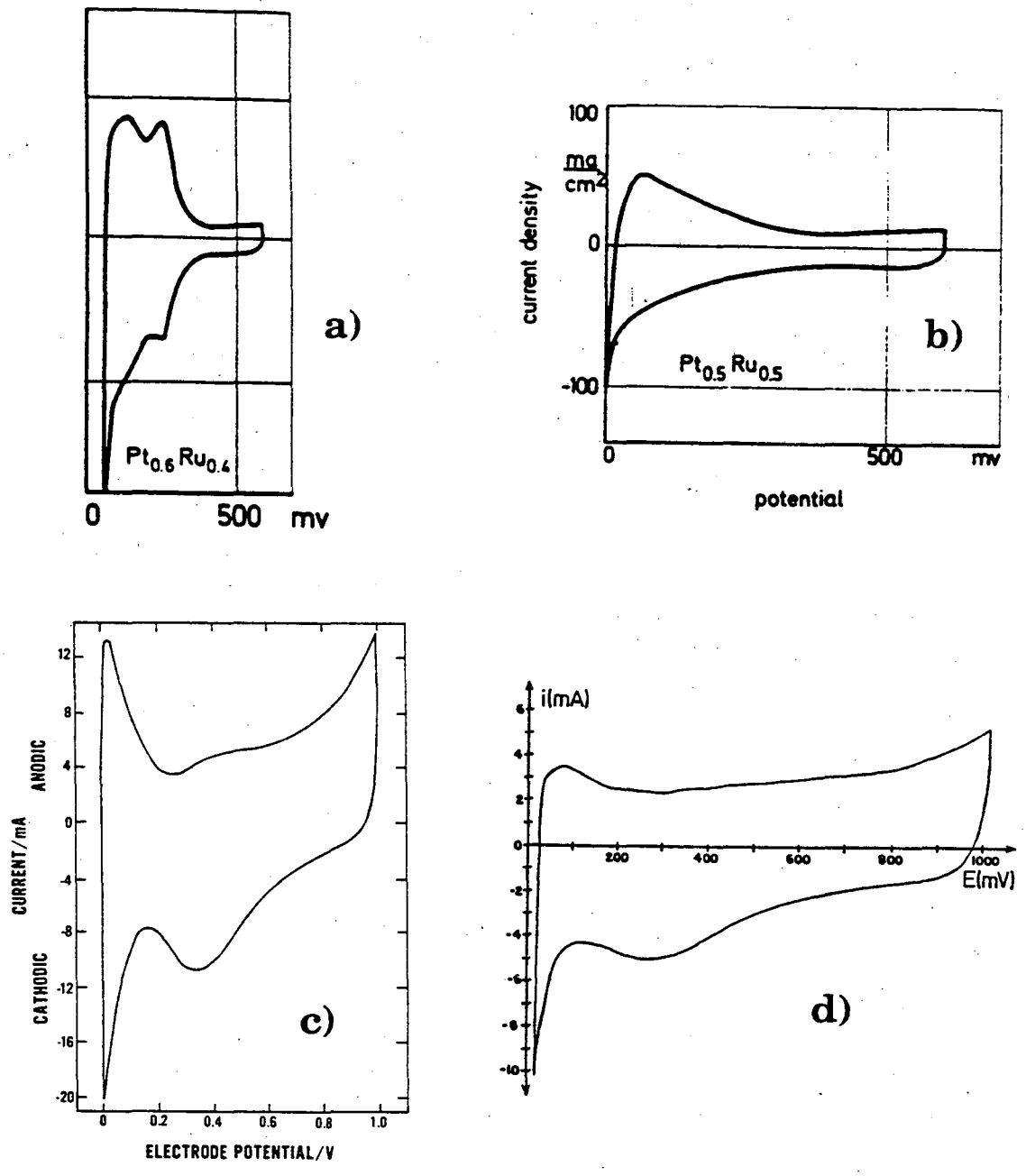

Figure 4-4. A comparison to cyclic voltammetry found in the literature shows similar features: loss of definition in the hydrogen region and higher double-layer capacitance region for Pt-Ru vs. Pt. a) Pt-Ru rolled sheets, 2000 mV/min, 3 N H_2SO_4 [25]; b) Raney Pt-Ru alloys, 40 mV/min, 3 N H_2SO_4 [25]; c) Pt-Ru/Cg, 14 mV/s, 1 M H_2SO_4 [68]; d) this work, Pt-Ru/Cg, 10 mV/s, 1 M H_2SO_4.

As mentioned before in the context of cyclic voltammetry on Pt-Ru alloys, Ru begins to form an oxide at potentials around 300 mV. This is also true of cyclic voltammetry on Ru alone, however, the properties of the oxide are a strong function of the upper potential encountered while sweeping. Up to approximately 1.0 V, the oxide formed is electrochemically reversible, *i.e.*, it is easily reduced upon returning the electrode to reducing potentials such as the H_2 open circuit region. However, upon exceeding 1.0 V (especially above 1.2 V), the Ru oxide becomes more tenacious and electrochemically irreversible [68]. The oxide can be chemically reduced by exposing it to a reducing atmosphere, *e.g.*, H_2 gas above 200 °C, after which time, the cyclic voltammogram will be characteristic of Ru in its reduced state. When alloyed with Pt, Ru can be taken to more oxidizing potentials (*e.g.*, 1.2 to 1.4 V), and the resulting oxide subsequently reduced upon cycling to H_2 open circuit. This has been attributed to the spillover of atomic hydrogen formed on Pt onto the oxidized Ru [68].

Additionally, it has been reported that dissolution of the Ru from Pt-Ru alloys occurs upon sweeping to oxidizing potentials resulting in a Pt-enriched alloy surface [50, 69]. As can be seen in Figure 4-5, cycling to 1500 mV has significantly altered the features of the i-V curve. The H_2 region has developed features characteristic of Pt, and the ratio of the double-layer charge to the H_2-desorption charge has decreased markedly. It is unclear, however, whether or not this is due to dissolution of Ru from the alloy, or alteration of the surface Ru species to an oxidized state.

Dramatic differences in the degree of wetting achieved by different methods can be seen in Figure 4-6. Both electrodes were fabricated with the same catalyst, catalyst loading, and reaction-layer PTFE content, and both

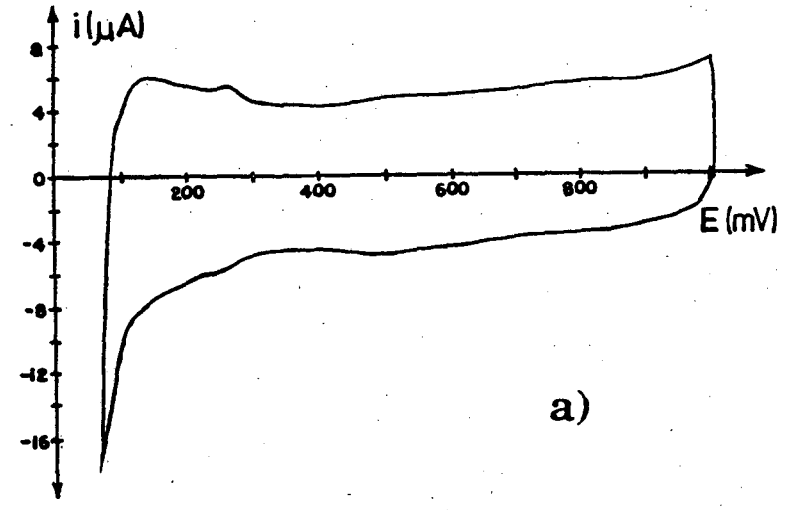

a)

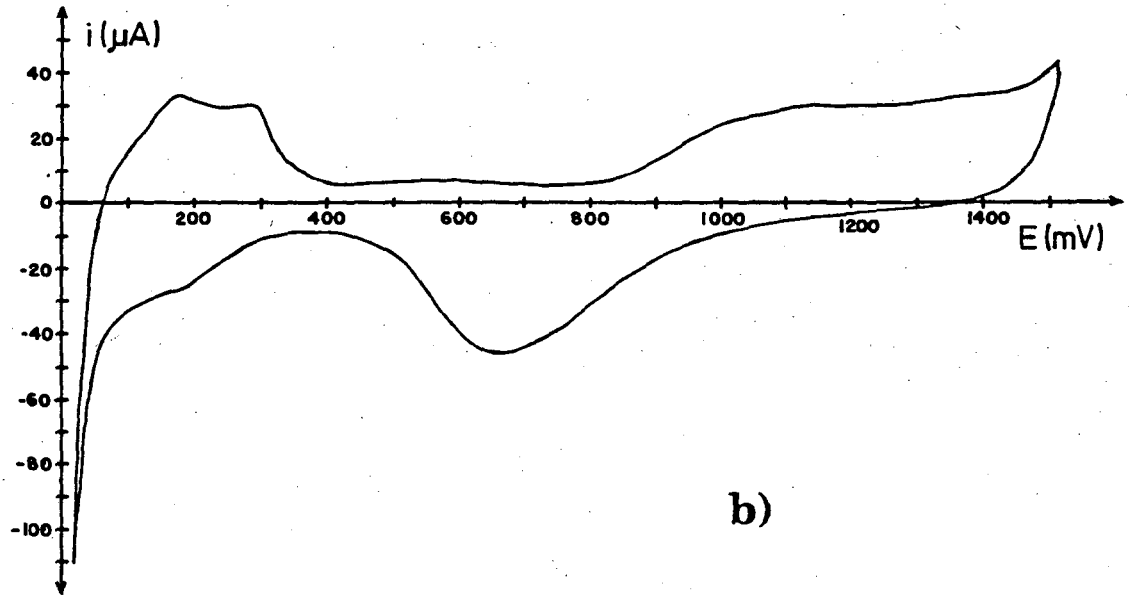

b)

4-5. Effect of cycling to different anodic potentials on the same electrode. a) 0 - 1000 mV, 100 mV/s; b) 0 - 1500 mV, 50 mV/s. Catalyst: 0.4 mg[Pt-Ru]/cm^2, 50 a/o Ru; 1 M H_2SO_4, 20 °C.

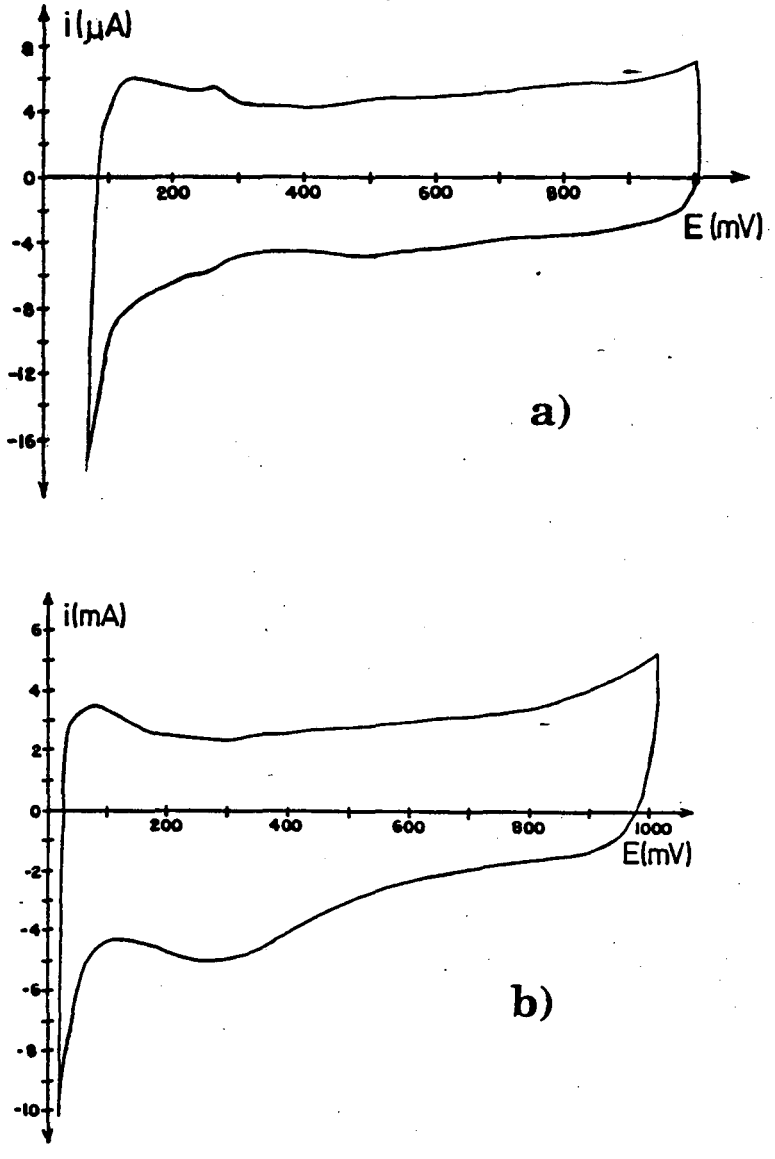

Figure4-6. Cyclic voltammograms indicating different degrees of wetting achieved with gas diffusion electrodes. Note: different current scales and different sweep rates. Both electrodes: 0.4 mg[Pt-Ru]/cm^2, 50 a/o Ru; 1 M H_2SO_4, 20 °C. a) soaked in electrolyte 24 hours, 100 mV/s; b) pre-treated with methanol on face before soaking in electrolyte 24 hours, 10 mV/s.

traces were taken under similar conditions. However, the electrode pre-treated with methanol (as discussed in Chapter 3) is characterized by currents three orders-of-magnitude higher than the one that was only soaked in the working electrolyte for twenty-four hours before cycling. The higher currents are indicative of a higher degree of wetting. This is not, however, a necessary indication of high performance, because a flooded reaction layer would show a large wetted area but low performance due to large diffusion losses in the pores.

An estimate of the catalyst surface area was made as shown in Figure 4-7. As described above, a double-layer capacitance "background" was estimated and subtracted from the anodic portion of the trace. The area under the curve, *i.e.*, up to 250 mV anodic to the potential at which hydrogen evolution was evident (the shaded area), was taken to be representative of the hydrogen desorption region. Assuming 210 mC/cm^2 for the adsorption of a monolayer of hydrogen on the catalyst surface, we calculated 123.8 cm^2/mg of Pt-Ru metal. This is higher than expected, but is within the normal range for Pt dispersed on high-surface-area carbon [36, 70].

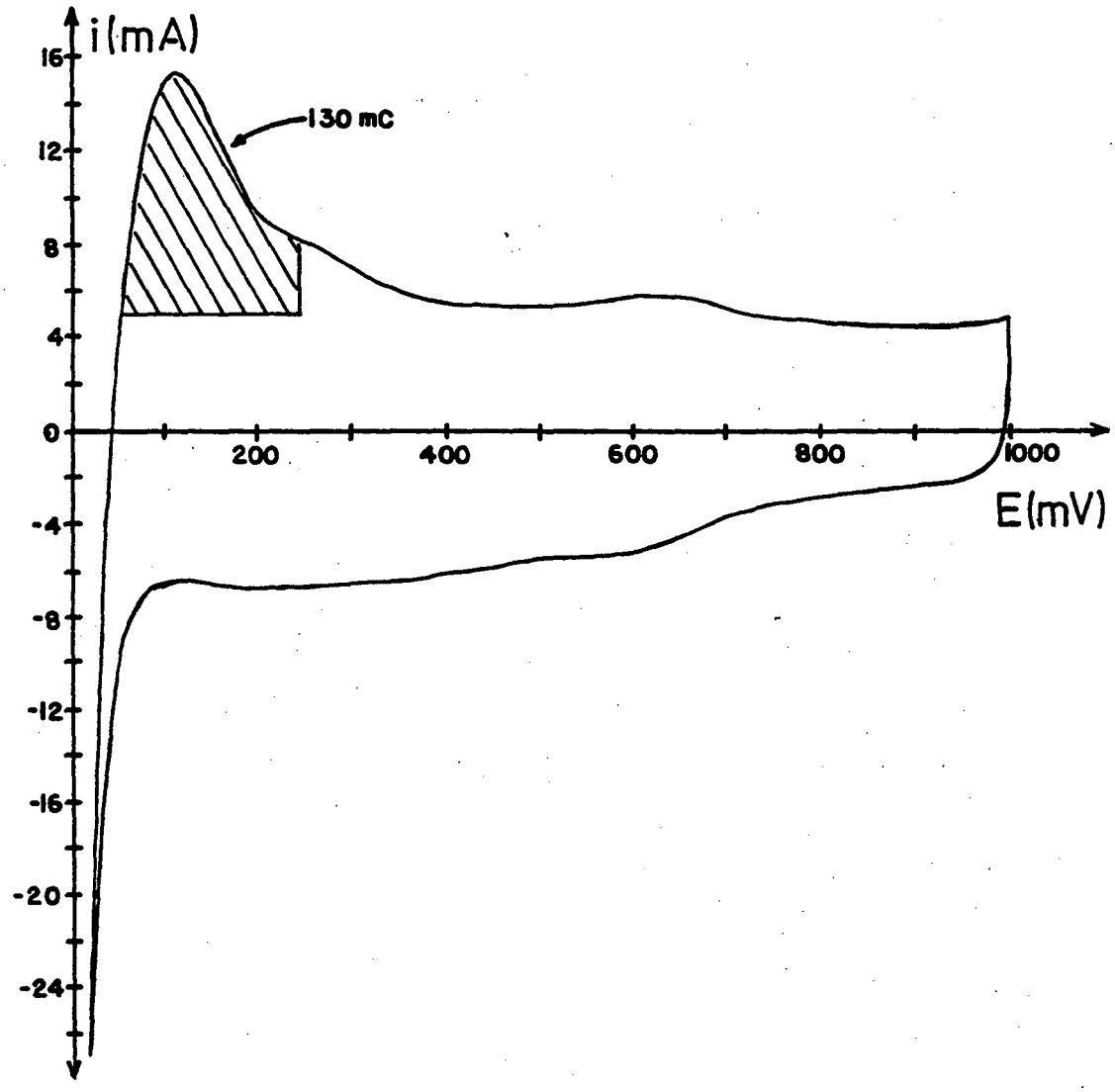

Figure 4-7. Determination of catalyst surface area. Catalyst loading: 0.4 mg[Pt-Ru, 50 a/o]/cm^2, 1 M H_2SO_4; 20 °C; 10 mV/s.

IR-Drop

IR-drop measurements were made as described in Chapter 3 (see p. 37). Figure 4-8 shows a representative result from such an experiment. The linear, nearly vertical section of the curve was interpreted as representative of voltage drop due to ohmic losses, and was calculated to be approximately 100 mΩ using Ohms Law.

IR-drop experiments carried out at other current densities, and in different electrolytes, revealed similar shapes and resulted in nearly equivalent values for the ohmic resistance. For the currents encountered during methanol oxidation, *i.e.*, less than 200 mA/cm^2, the IR losses will amount to less than 20 mV. Polarization curves reported in this work, therefore, were not IR-corrected.

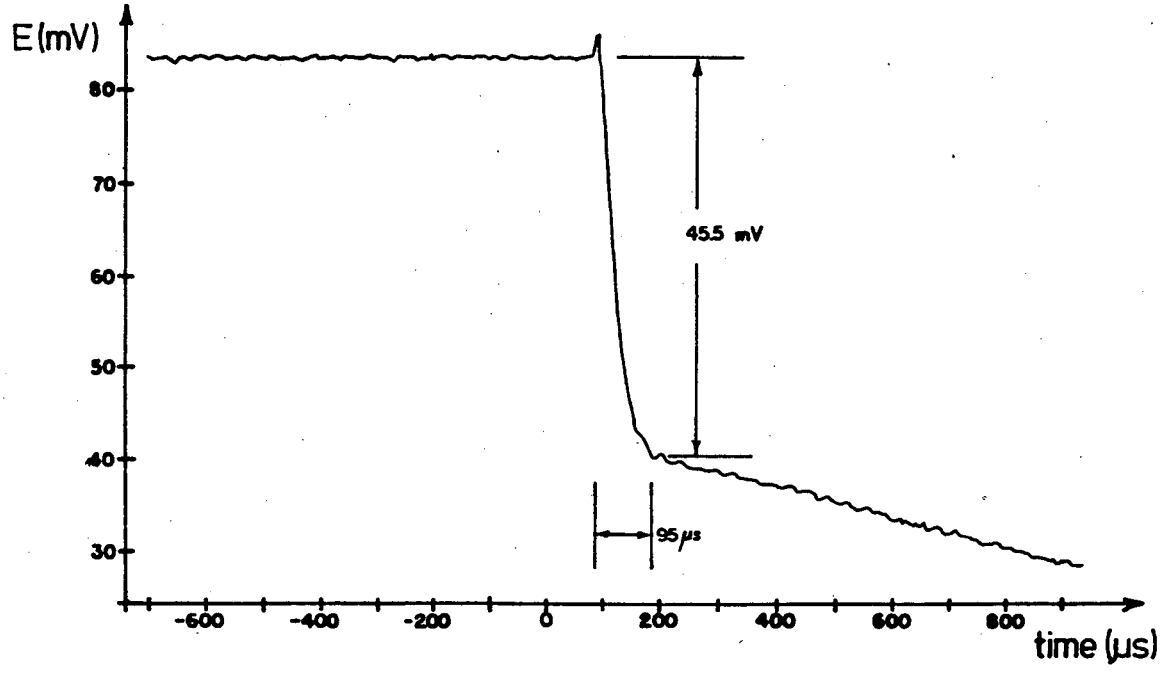

Figure 4-8. IR-drop experiment using the current interrupt method. 5 ms sampling rate; 1 M H_2SO_4; 50 °C; I = 400 mA.

Methanol Oxidation on Platinum/Ruthenium

Effect of Catalyst Composition

The main thrust of this thesis was to examine and optimize the electrode macro-structure for methanol oxidation on supported Pt-Ru catalyst. It was of interest, however, as an internal check, to compare methanol oxidation on supported Pt with Pt-Ru for identically fabricated electrodes, using similarly produced electrocatalysts. Results by others using Pt-Ru in acidic media have shown substantial improvements in performance with decreases in overpotential by about 140 mV with respect to Pt alone [25]. It was expected that increased performance would also occur in carbonate electrolytes using supported Pt-Ru.

Figure 4-9 shows results for methanol oxidation in cesium carbonate, revealing that an electrode with Pt-Ru catalyst shows markedly lower overpotential vs. a similar Pt catalyst. All physical parameters between the two tests were the same except the catalyst loading. The Pt catalyst was made as 10 wt% Pt on graphitized Vulcan XC-72R; the Pt-Ru catalyst as 5 wt% Pt-Ru on graphitized Vulcan. To keep all other parameters as close as possible between the two electrodes (*e.g.*, reaction layer thickness), the Pt-catalyzed electrode has a loading of 1 mg[total metal]/cm^2 and the Pt-Ru catalyzed electrode has a loading of 0.4 mg[total metal]/cm^2. These results are consistent with comparable studies in acidic electrolytes.

There have only been few performance studies of methanol oxidation on Pt-Ru using vaporized methanol on a gas diffusion electrode. Of particular note are the results of Cairns *et al* [6]., Giner *et al.*[8], and

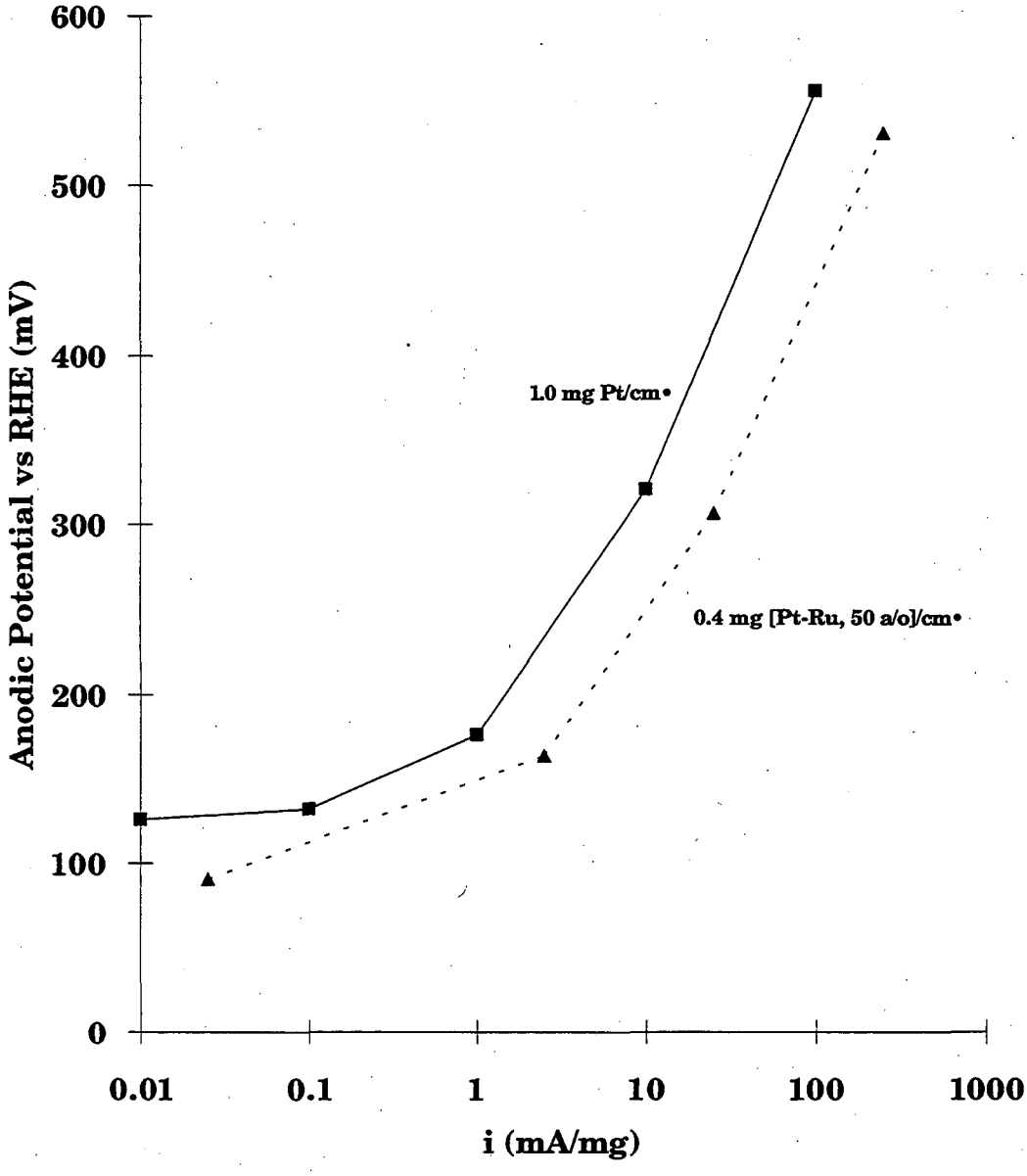

Figure 4-9. Comparison between methanol oxidation on Pt and Pt-Ru on a mass-specific basis. 120 °C, 72 wt% Cs_2CO_3, 20 w/o PTFE in the reaction layer .

Landsman and Luczak [71], each of whom operated full fuel cells with air or oxygen cathodes. As discussed earlier, the study by Cairns *et al.* was very similar to this work, differing mainly in the catalyst; Cairns *et al.* used a Pt-black catalyst with a loading of approximately 35 mg/cm^2. The work of Giner *et al.*, which is also similar to the present effort, utilized 0.5 mg/cm^2 Pt dispersed on carbon as catalyst; however, their gaseous fuel stream was composed of 26 % methanol, 29 % water, and 45 % nitrogen, and they operated at temperatures of 150 to 180 °C, and pressures on the order of 120 psig. Landsman *et al.* operated their system using concentrated phosphoric acid (98 %) at 200 °C with Pt-Ru supported on carbon at [0.5 mg Pt/0.078 mg Ru]/cm^2. All three references are compared to present work in Figure 4-10, with current densities on a specific electrocatalyst mass basis for direct comparison of performance. Note that the present work on Pt-Ru supported catalyst in cesium carbonate compares favorably with the work by Giner *et al.*, although they operated 30 °C higher, and indicates the advantage of Pt-Ru catalyst over Pt, allowing operation at up to 30 °C lower at equivalent levels of performance. This work shows the highest methanol oxidation performance to date and demonstrates the significant benefit of operating with concentrated cesium carbonate electrolyte and supported Pt-Ru electrocatalyst.

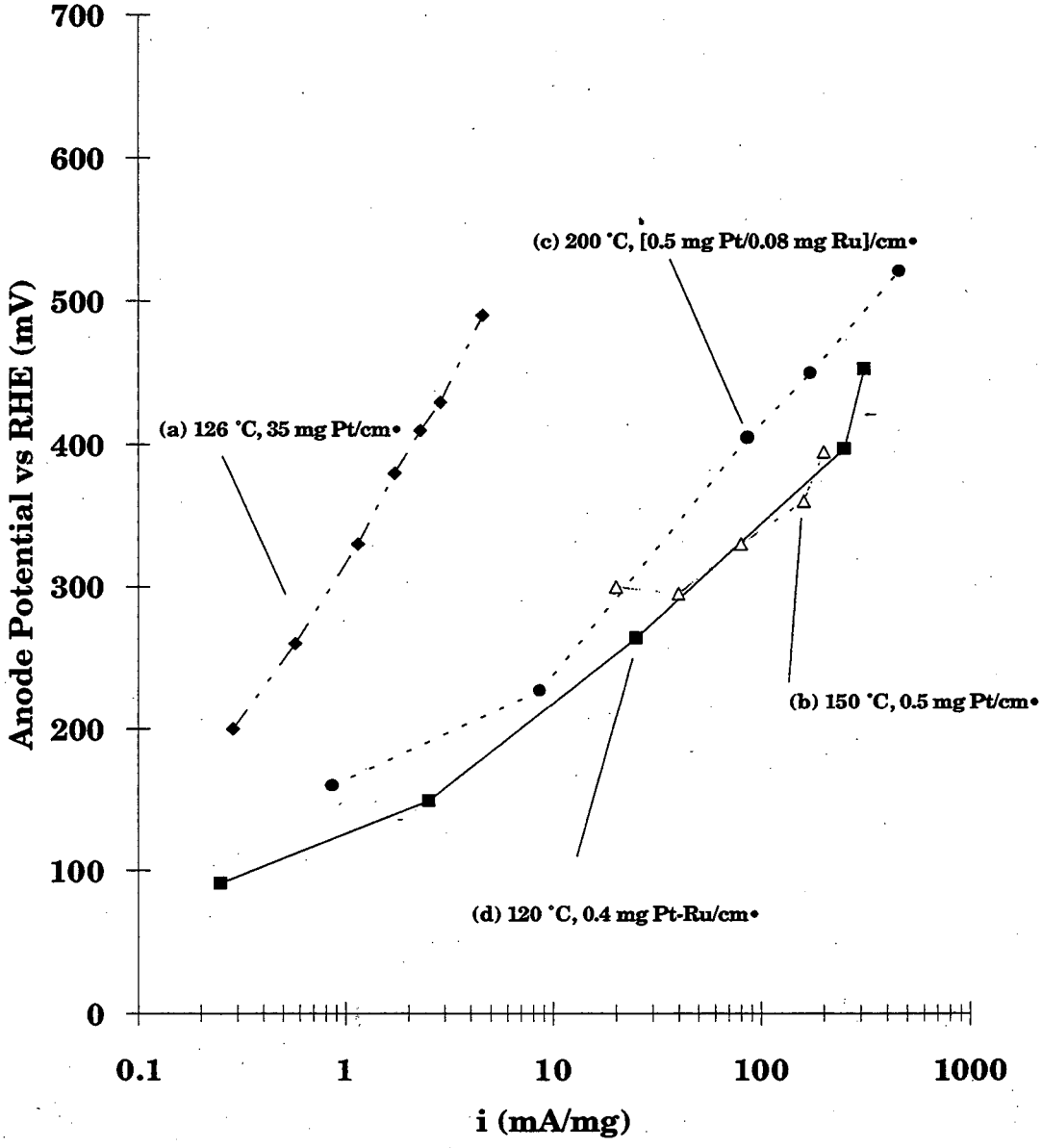

Figure 4-10. Performance of present work vs. literature. a) Cairns *et al.*, conc. cesium carbonate, Pt-black; b) Giner *et al.*, conc. cesium carbonate, Pt supported on carbon; c) Landsman *et al.*, conc. H_3PO_4, Pt-Ru on carbon; d) this work, conc. cesium carbonate, Pt-Ru on graphitized carbon.

Effect of Temperature on Performance

Assuming Arrhenius behavior, the activation energy of a reaction (E_A) is related to the reaction rate (*i.e.*, the current density, i) as

$$\ln(i) = \ln(A) - \frac{E_A}{RT} \qquad [4\text{-}1]$$

A plot of ln(i) vs. 1/T will therefore give a slope of $-E_A/R$. A performance curve for methanol oxidation on Pt-Ru in concentrated cesium carbonate is shown in Figure 4-11 at three temperatures sufficiently below the boiling point of the electrolyte and at a potential at which diffusion has not become a significant fraction of the overpotential. A cross plot is shown in Figure 4-12, which gives an activation energy of 77 kJ/mol. This is substantially higher than that reported by Cameron *et al.* [37], who report for oxidation of methanol on Pt and Pt-Ru catalysts activation energies of 36 kJ/mol and 49 kJ/mol, respectively. Unfortunately, they do not report the electrolyte or fuel composition used in determining these values. Many of their reported polarization curves are in 3 M H_2SO_4, and methanol was normally in solution at a concentration of approximately 1 mol/liter. Although one cannot infer from the higher activation energy a higher activity for methanol oxidation in cesium carbonate than in acids, one can assert that temperature has a more dramatic effect on performance in cesium carbonate. Results by Giner *et al.* for methanol oxidation on Pt in concentrated cesium carbonate [8] are shown in Figure 4-12 for comparison, though it is difficult to determine a slope from the points.

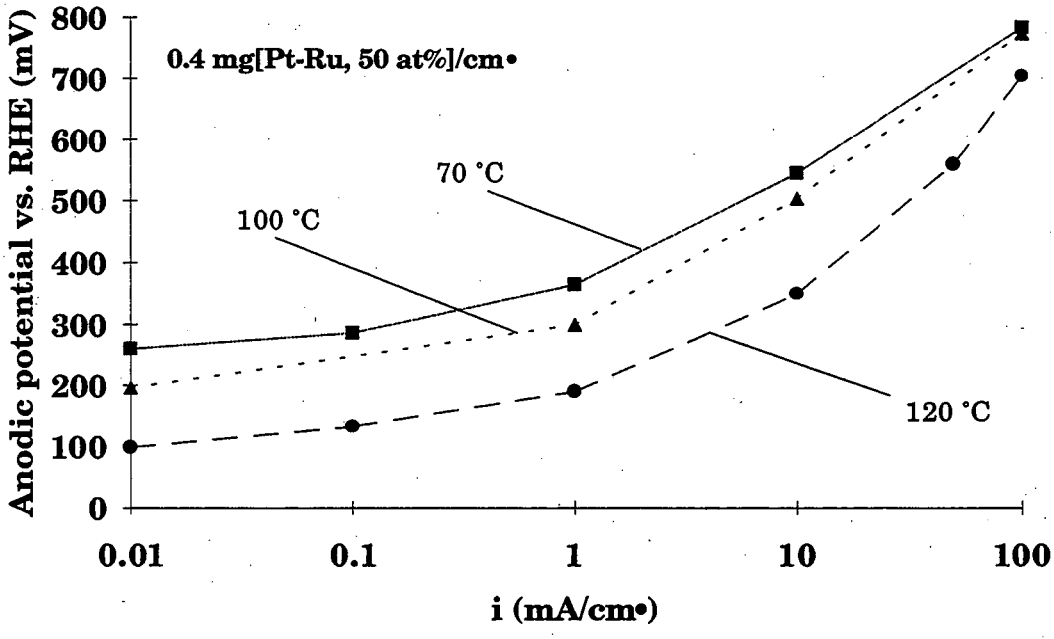

Figure 4-11. Polarization curve for oxidation of methanol on (Pt-Ru)-supported gas diffusion electrode. Reaction layer at 30 w/o PTFE.

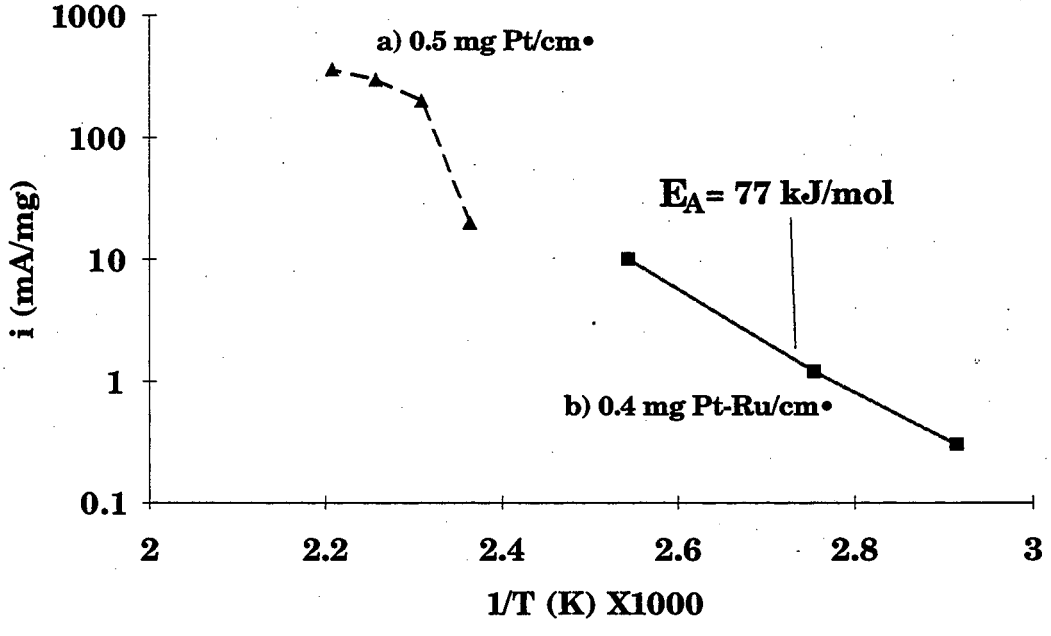

Figure 4-12. Natural log of current as a function of temperature to determine the activation energy for oxidation of methanol on Pt-Ru in concentrated cesium carbonate. Values are taken at anode potentials of 300 mV vs. RHE. a) Giner *et al.* [8]; b) this work, 50 a/o Ru.

Some additional performance curves are shown in Figure 4-13, for 40 and 20 w/o PTFE. There are several important points to make concerning these graphs. First, note that the current density scale for the 40 w/o PTFE electrode is one-tenth that of the 20 w/o electrode. The effect of PTFE content in the reaction layer is discussed in the following section. Also, the performance for these systems does not increase directly with temperature, as would be expected from the previous examination of the activation energies. Indeed, both electrodes show a maximum in the performance as a function of temperature. This can be attributed to the effects of diffusion limitation effects. As the system is taken close to the boiling point of the electrolyte, the vapor pressure of the water in the electrolyte becomes appreciable and its effect on the diffusion of fuel and products is no longer negligible. As reported in the work of Cairns *et al.* [6], optimum performance is found when operating at 10 to 15 °C below the boiling point of the electrolyte, which is approximately 140 °C in this work.

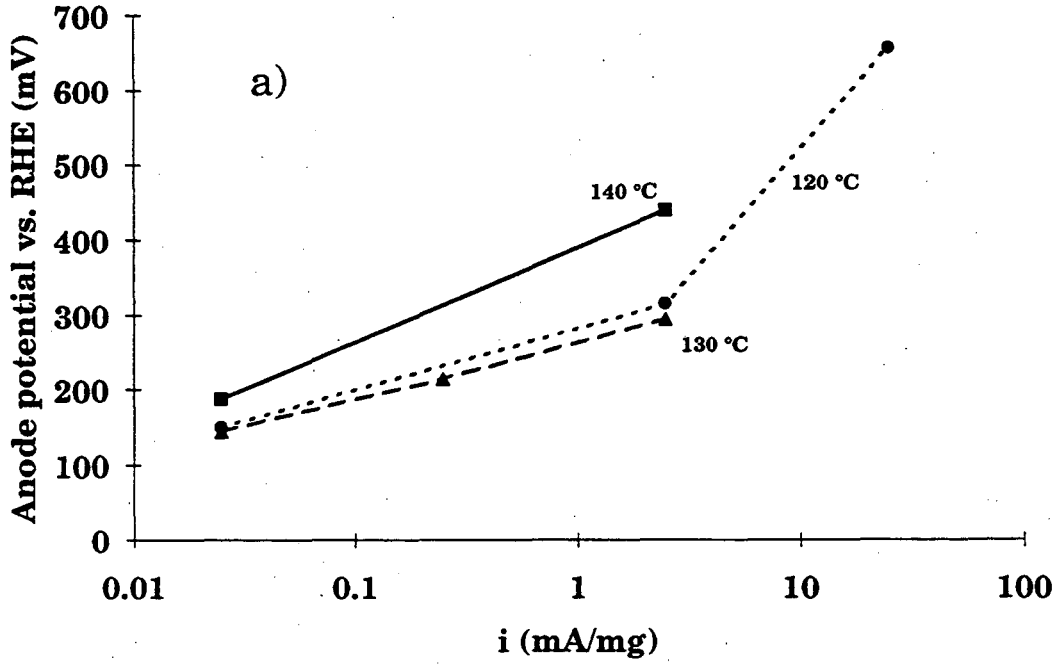

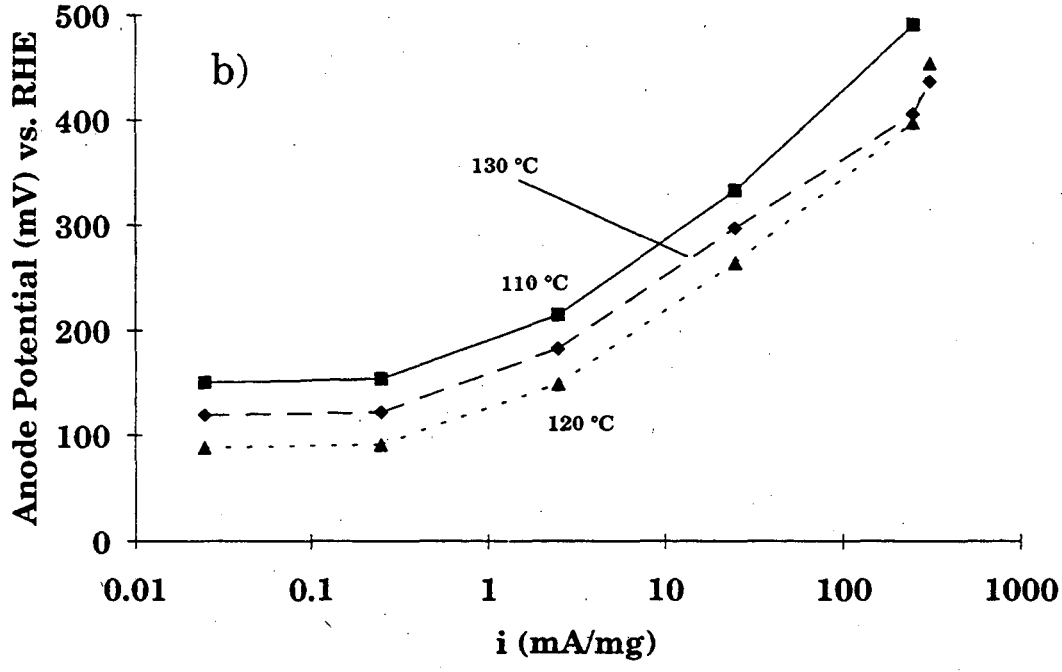

Figure 4-13. Performance for methanol oxidation on supported Pt-Ru gas diffusion electrode. Loading: 0.4 mg[Pt-Ru, 50 a/o]/cm^2; conc. cesium carbonate; a) 40 w/o PTFE, b) 20 w/o PTFE.

Effect of Teflon Content on Performance

In an effort to control the wetting characteristics of the electrodes, the PTFE content in the reaction layer was varied from 15 w/o up to 40 w/o. Polarization experiments were performed on these electrodes, at several temperatures, in an effort to determine the optimum PTFE content, and, therefore, the optimum wetting of the reaction layer. Some results of these performance tests are shown in Figure 4-14 (a) and (b), for temperatures of 120 and 130 °C, respectively. A cross-plot was generated from these two plots by taking the current density at 400 mV for each of the curves and plotting the current density vs. the PTFE content, as shown in Figure 4-15. Electrodes were not fabricated with 25 w/o PTFE in the reaction layer, however, the curve reveals a maximum in performance in the region of 20 to 30 w/o, possibly at 25 w/o. This is in close agreement with results in the literature for methanol oxidation in acidic electrolytes [14, 16, 72, 73]. It is interesting to note that, in both Figure 4-14 (a) and (b), the curves for 20 w/o and 30 w/o PTFE do cross. However, a cross plot generated from current densities at 300 mV would be similar to that at 400 mV, although the optimum PTFE content might be skewed more toward 30 w/o PTFE.
As discussed in Chapter 2, the gas diffusion electrode performance is sensitive to the distribution of electrolyte in the reaction layer. A balance must be struck between sufficient wetting (to maintain access to as much catalyst surface as possible) and short diffusion pathways for the fuel and products. Poor performance of the electrodes with the extreme values, low and high, of PTFE content can be attributed directly to the wetting characteristics of the reaction layer . At 15 w/o, the low PTFE content has resulted in lowered hydrophobicity and allowed the reaction layer to be

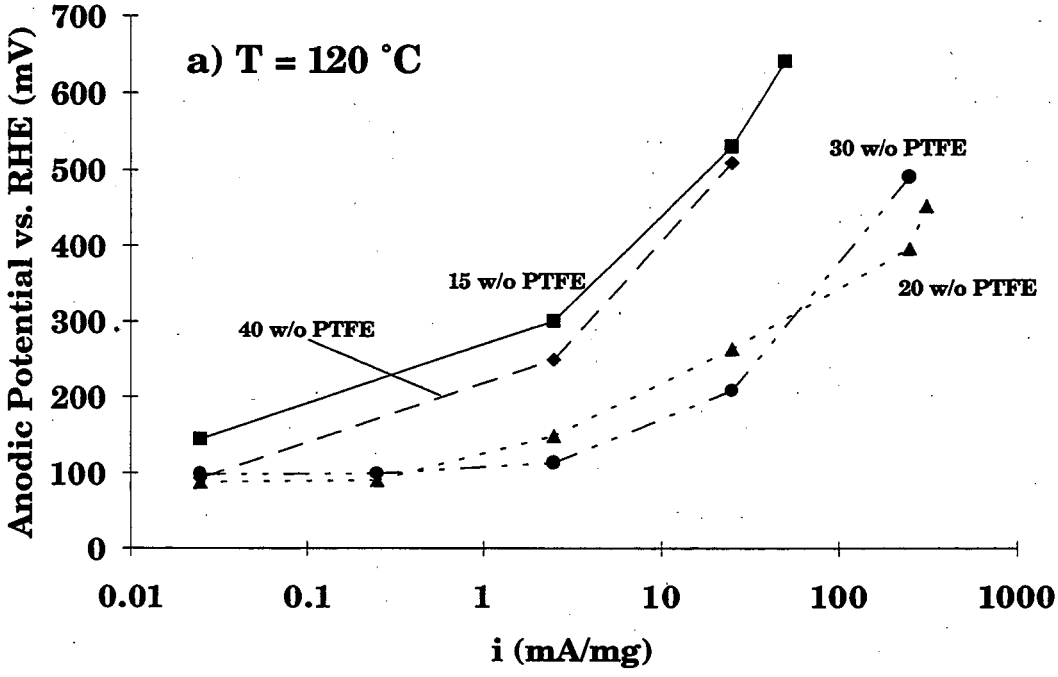

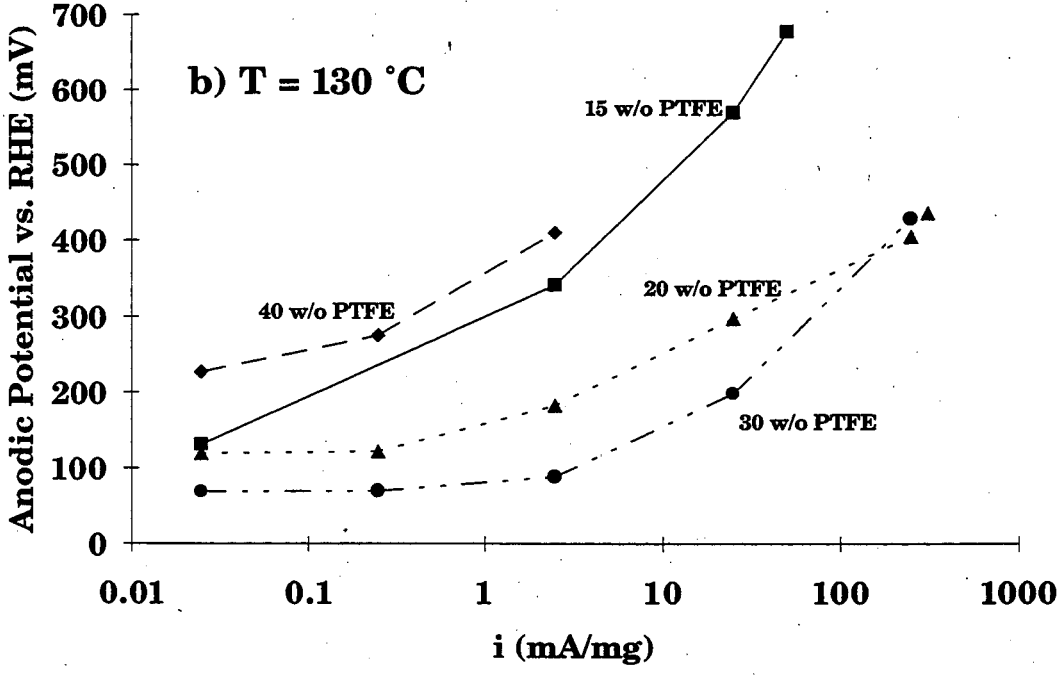

Figure 4-14. Performance as a function of PTFE content in the reaction layer for methanol oxidation on a gas diffusion electrode at a) 120 °C, b) 130 °C. 0.4 mg[Pt-Ru 50 a/o]/cm^2; concentrated cesium carbonate.

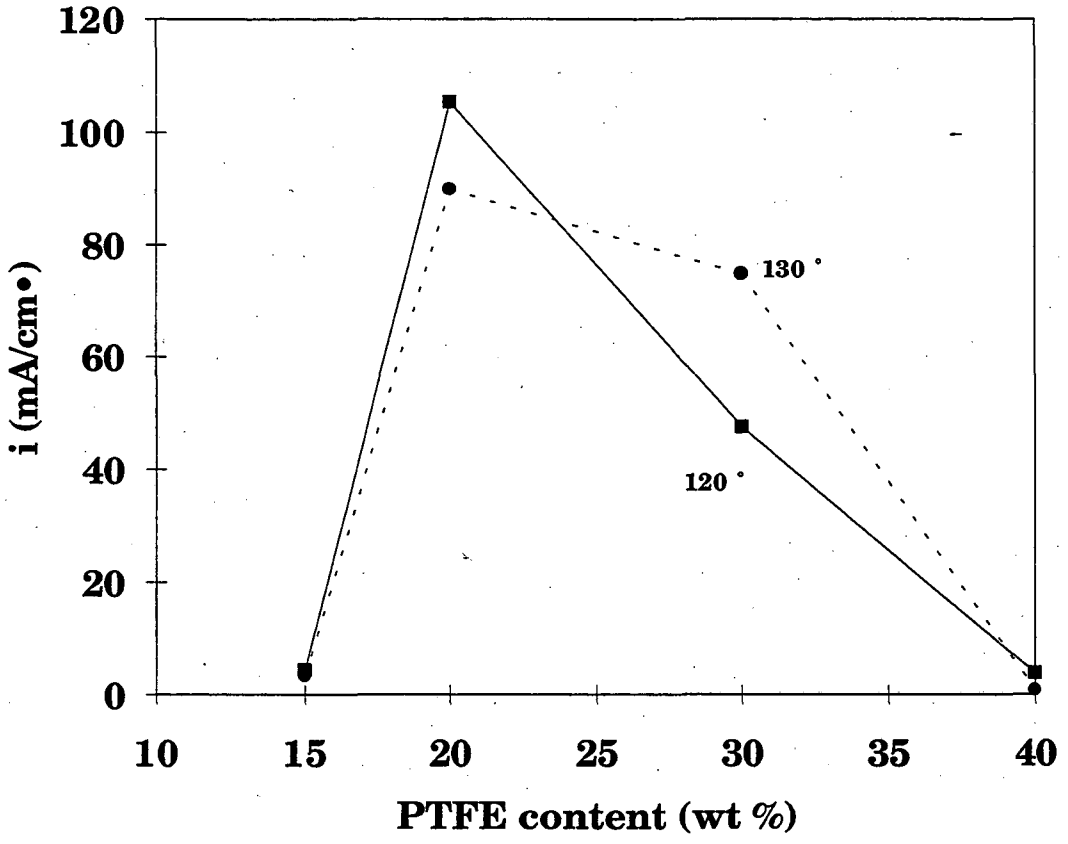

Figure 4-15. Current density vs. teflon content for methanol oxidation on Pt-Ru supported gas diffusion electrodes. concentrated cesium carbonate; E = 400 mV (vs. RHE); 0.4 mg[Pt-Ru, 50 a/o]/cm^2.

flooded. The greater wetting has increased the effective diffusion path length, thereby inhibiting the transport of fuel to and products away from the catalyst sites and reducing the limiting current, which is diffusion controlled. Conversely, too much PTFE, as in the case of the 40 w/o electrode, has left pores unwetted and catalyst sites inaccessible. The optimum PTFE content allows access to a maximum amount of catalyst while minimizing the effective diffusion path length of dissolved and ionic species.

Chapter 5. Conclusions and Recommendations

Pt-Ru supported on graphitized carbon demonstrated a marked increase in performance over supported Pt for the oxidation of methanol in concentrated cesium carbonate electrolytes. This is reassuring because similar results have been found by others in acidic media. Indeed, performance curves (on a per milligram of total metal basis) recorded here on Pt-Ru at 120 °C match or exceed performance by others on Pt-black or supported Pt in concentrated cesium carbonate at 120 to 150 °C [6, 8], and on supported Pt-Ru in concentrated H_3PO_4 at 200 °C as reported by Landsman and Luczak [71]. In fact, the performance results in this work are higher than any reported in literature to date.

The reaction-layer structure is critical to the performance of a gas diffusion electrode. As others have found, the PTFE content in the reaction layer, and consequently the extent of wetting, shows a marked effect on performance. Experiments in this work, in which the PTFE content of the reaction layer was varied from 15 to 40 w/o, follow the patterns reported in the literature. Low performance at 15 w/o PTFE is attributed to flooding of the reaction layer pores, specifically to the deleterious effect on diffusion rate of reactants and products to and from the catalyst surface. Poor performance was also experienced at the high loading of 40 w/o PTFE, attributed simply to an overly hydrophobic reaction layer, and inaccessible catalyst sites. An optimum has been found, in this case between 20 and 30 wt% PTFE, which is

comparable to that found by Goodenough *et al.* [72, 73] at 27 wt%, but slightly lower than that found by Watanabe *et al.* [14, 16] at 30%.

With all PTFE content levels in the reaction layer, it was found that performance, as a function of temperature, passed through a maximum, specifically at 10 to 15 °C below the boiling point of the electrolyte. This is seemingly in contrast to expectations that performance will continue to increase with increasingly temperature, as a plot of the activation energy would suggest. However, the decrease in performance as the temperature approaches the boiling point of the electrolyte is attributed to an increase in the water vapor pressure, which inhibits diffusion of the fuel and reaction products in the gas phase.

Characterization of the catalyst by XRD revealed a strong Pt signal and a weaker, but significant, Ru-rich alloy signal, while cyclic voltammetry indicated a strong Ru presence in the catalyst surface. This may possibly be explained by enrichment of the catalyst surface (several atomic layers deep) by Pt due to the extensive exposure to a hot, reducing atmosphere during manufacture of the catalyst, and the subsequent enrichment by Ru due to exposure to an oxidizing atmosphere while sintering the electrode. McNicol *et al.*, in their study on the effect of activation conditions on Pt-Ru alloys, report surface enrichment of Pt with exposure to H_2 and enrichment of Ru with exposure to air or O_2 [54].

Further studies of the catalyst would be helpful in resolving the differences in results between the two types of characterization used in this work. Certainly XRD of the catalyst during stages in the manufacture of gas diffusion electrodes and their subsequent use in polarization experiments might reveal changes in surface and bulk composition of the alloy. A better understanding of when (and if) the structure changes can lead to

modifications of and more control of the catalyst and electrode manufacturing processes.

It would be informative to monitor the composition of the fuel outlet gases to determine whether the methanol oxidizes completely to CO_2, and to identify parameter values that may maximize fuel conversion efficiency. Previous work by Cairns *et al.* [6] showed through gas chromatography, and subsequent closed mass balances, that all of the reacted methanol could be accounted for as product CO_2. Although the present work is similar to that of Cairns, the effect of the bimetallic catalyst on the extent of the reaction should be considered.

The co-precipitation method for preparing the catalyst in this work was selected for its simplicity and an extensive body of work that has utilized it as a means of preparing active, well-characterized supported catalysts. There have been many other methods developed recently, which are claimed to give supported catalysts of higher activity than the method selected by the authors. It would certainly be of interest to utilize, and study, these catalysts in the system described herein. Additionally, the composition of the catalyst used in this investigation (*i.e.*, Pt-Ru at 1:1 atomic ratio) may possibly be further optimized for the methanol-cesium carbonate system.

References

1. Kinoshita, K., McLarnon, F. R., and Cairns, E.J., *Fuel Cell Handbook*, Prepared for the U.S. Dept. of Energy, Office of Fossil Energy (1988).
2. Kordesch, K., Reindl, M., "Fuel Cells," *Electrochemical Reactors: Their Science and Technology. Part A: Fundamentals, Electrolysers, Batteries and Fuel Cells*," ed. M.I. Ismail, Elsevier Science Publishers B.V., Amsterdam, 1989, p. 450.
3. Liebhafsky, H.A., Cairns, E.J., *Fuel Cells and Fuel Batteries*, John Wiley & Sons, New York (1969).
4. Srinivasan, S., "Fuel Cells for Extraterrestrial and Terrestrial Applications," *J. Electrochem. Soc.*, **136**, 41 (1989).
5. Kordesch, K., "The Advancement of Fuel Cell Systems and Spin-off Battery Technology," *Ber. Bunsenges. Phys. Chem.*, **94**, 902 (1990).
6. Cairns, E.J., and Bartosik, D.C., "A Methanol Fuel Cell with an Invariant Alkaline Electrolyte," *J. Electrochem. Soc.*, **111**, 1205 (1964).
7. Rupich, M.M.W., Brummer, S.B., Galligan, D.A., Kingsley, S.C., and Mardis, E.L., "Catalysis of Direct Methanol Electro-Oxidation in Buffered Electrolytes," DOE:DE-ACO2-83ER13066, Final Report to U.S. Dept. of Energy by EIC Labs (1987).
8. Sarangapani, S., Lessner, P., Manoukian, M., Kosek, J., Bombard, T., and Giner, J., "Methanol Fuel Cell, Progress for the period 8/16/89 to 1/9/90," US-DOE SBIR P, 1 (1990); also, Abstract #36, presented at 181st Meeting of the Electrochemical Society, St. Louis, MO (1992).

9. Fritts, S.D., and Sen, R.K., "Assessment of Methanol Electro-Oxidation for Direct Methanol-Air Fuel Cells," PNL-6077, Prepared for the U.S. Dept. of Energy by Pacific Northwest Laboratory under Contract DE-AC06-76RLO 1830 (1988).

10. Verbrugge, M.W., "Methanol Diffusion in Perfluorinated Ion-Exchange Membranes," *J. Electrochem. Soc.*, **136**, 417 (1989).

11. Niedrach, L.W., and Alford, H.R., "A New High-Performance Fuel Cell Employing Conducting-Porous-Teflon Electrodes and Liquid Electrolytes," *J. Electrochem. Soc.*, **112**, 117 (1965).

12. Kordesch, K., Gsellmann, J., Jahangir, S., and Schautz, M., in *Proceedings of the Symposium on Porous Electrodes: Theory and Practice*, Edited by H.C. Maru, T. Katan, and M.G. Klein, The Electrochemical Society, Inc., Pennington, NJ, 1984, p. 163.

13. Motoo, S., Watanabe, M., and Furuya, N., "Preliminary note: Gas Diffusion Electrode of High Performance," *J. Electroanal. Chem.*, **160**, 351 (1984).

14. Watanabe, M., Tomikawa, M., and Motoo, S., "Preliminary note: Preparation of a High Performance Gas Diffusion Electrode," *J. Electroanal. Chem.*, **182**, 193 (1985).

15. Watanabe, M., Tozawa, M., and Motoo, S., "Preliminary note: A Gas Diffusion Electrode for Oxygen Reduction Working at 100% Utilization of Catalyst Clusters," *J. Electroanal. Chem.*, **183**, 391 (1985).

16. Watanabe, M., Tomikawa, M., and Motoo, S., "Experimental Analysis of the Reaction Layer Structure in a Gas Diffusion Electrode," *J. Electroanal. Chem.*, **195**, 81 (1985).

17. Watanabe, M., Makita, K., Usami, H., and Motoo, S., "New Preparation Method of a High Performance Gas Diffusion Electrode Working at 100% Utilization of Catalyst Clusters and Analysis of the Reaction Layer," *J. Electroanal. Chem.*, **197**, 195 (1986).

18. Wilson, M.S. and Gottesfeld, S., "High Performance Catalyzed Membranes of Ultra-low Pt Loadings for Polymer Electrolyte Fuel Cells," *J. Electrochem. Soc.*, **139**, L28 (1992).

19. Paik, W., Springer, T.E., and Srinivasan, S., "Kinetics of Fuel Cell Reactions at the Platinum/Solid Polymer Electrolyte Interface," *J. Electrochem. Soc.*, **136**, 644 (1989).

20. Watanabe, M., Uchida, M., and Motoo, S., "Applications of the Gas Diffusion Electrode to a Backward Feed and Exhaust (BFE) Type Methanol Anode," *J. Electroanal. Chem.*, **199**, 311 (1986).

21. Furuya, N., and Motoo, S., "Application of the Gas Diffusion Electrode of High Performance to Methanol Fuel Cells," *J. Electroanal. Chem.*, **179**, 303 (1984).

22. Watanabe, M., Uchida, M., and Motoo, S., "Preparation of Highly Dispersed Pt + Ru Alloy Clusters and the Activity for the Electrooxidation of Methanol," *J. Electroanal. Chem.*, **229**, 395 (1987).

23. Cairns, E.J., and McInerney, E.J., "High Activity Platinum Electrocatalysts for the Direct Anodic Oxidation of Saturated Hydrocarbons," *J. Electrochem. Soc.*, **114**, 980 (1967).

24. Cairns, E.J., and Paynter, J., "Electrocatalysts for the Direct Electrochemical Oxidation of n-Octane in Fuel Cells," *J. Electrochem. Soc.*, **114**, 1218 (1968).

25. Binder, H., Köhling, A., and Sandstede, G., "Effect of Alloying Components on the Catalytic Activity of Platinum in the Case of Carbonaceous Fuels," *From Electrocatalysis to Fuel Cells*, ed. G. Sandstede, Univ. Washington Press, Seattle, 1972, p. 43.

26. Bagotzky, V.S., and Vassilyev, Yu.B., "Mechanism of Electro-Oxidation of Methanol on the Platinum Electrode," *Electrochim. Acta*, **12**, 1323 (1967).

27. Bagotzky, V.S., Vassiliev, Yu.B., and Khazova, O.A., "Generalized Scheme of Chemisorption, Electrooxidation and Electroreduction of Simple Organic Compounds on Platinum Group Metals," *J. Electroanal. Chem.*, **81**, 229 (1977).

28. McNicol, B.D., "The Electrocatalytic Aspects of Direct Oxidation of Methanol for Fuel Cells Applications," Proceedings of the Workshop on the Electrocatalysis of Fuel Cell Reactions, **79-2**, 93 (1978).

29. Hampson, N.A., Willars, M.J., and McNicol, B.D., "Study of the Methanol Oxidation Reaction on Platinum Using the Potential-Step Technique," *JCS. Faraday I*, **75**, 2535 (1979).

30. Willsau, J., Wolter, O., and Heitbaum, J., "On the Nature of the Adsorbate During Methanol Oxidation at Platinum. A DEMS Study," *J. Electroanal. Chem.*, **185**, 163 (1985).

31. Wolter, O., Willsau, J., and Heitbaum, J., "Reaction Pathways of the Anodic Oxidation of Formic Acid on Pt Evidenced by ^{18}O Labeling--A DEMS Study," *J. Electrochem. Soc.*, **7**, 1635 (1985).

32. Parsons, R., and VanderNoot, T., "The Oxidation of Small Organic Molecules. A Survey of Recent Fuel Cell Related Research," *J. Electroanal. Chem.*, **257**, 9 (1988).

33. Leger, J.M., and Lamy, C., "The Direct Oxidation of Methanol at Platinum Based Catalytic Electrodes: What is New Since Ten Years?" *Ber. Bunsenges. Phys. Chem.*, **94**, 1021 (1990).

34. Vielstich, W., Christensen, P.A., Weeks, S.A., and Hamnett, A., "Preliminary Note: Evidence for COH as an Adsorbed Intermediate in the Anodic Oxidation of Methanol by ECDTMS and SNIFTIRS," *J. Electroanal. Chem.*, **242**, 327 (1988).

35. Christensen, P.A., Hamnett, A., and Weeks, S.A., "*In-Situ* IR Study of Adsorption and Oxidation of Methanol on Platinum and Platinised Glassy Carbon Electrodes in Sulphuric Acid Solution," *J. Electroanal. Chem.*, **250**, 127 (1988).

36. McNicol, B.D., "Electrocatalytic Problems Associated with the Development of Direct Methanol-Air Fuel Cells," *J. Electroanal. Chem.*, **118**, 71 (1981).

37. Cameron, D.S., Hards, G.A., Harrison, B., and Potter, R.J., "Direct Methanol Fuel Cells: Recent Developments in the Search for Improved Performance," *Platinum Metals Rev.*, **31**, 173 (1987).

38. Cathro, K.J., "The Use of Pt-Re Catalysts for the Oxidation of Aqueous Methanol," *Electrochem. Tech*, **5**, 441 (1967).

39. McKee, D.W., and Scarpellino, A.J. Jr., "Electrocatalysts for Hydrogen/Carbon Monoxide Fuel Cell Anodes. III. The Behavior of Supported Binary Noble Metals," *Electrochem. Tech.*, **6**, 101 (1968).

40. Ross, P.N., Kinoshita, K., Scarpellino, A.J., and Stonehart, P., "Electrocatalysis on Binary Alloys. II: Oxidation of Molecular Hydrogen on Supported Pt + Ru Alloys," *J. Electroanal. Chem.*, **63**, 97 (1975).

41. Goodenough, J.B., Hamnett, A., Kennedy, B.J., Manoharan, R., and Weeks, S.A., "Methanol Oxidation on Unsupported and Carbon Supported Pt+Ru Anodes," *J. Electroanal. Chem.*, **240**, 133 (1988).

42. Goodenough, J.B., and Manoharan, R., "Intraalloy Electron Transfer and Catalyst Performance: A Spectroscopic and Electrochemical Study," *Chemistry of Materials*, **1**, 391 (1989).

43. Swathirajan, S., and Mikhail, Y.M., "Electrochemical Oxidation of Methanol at Chemically Prepared Platinum-Ruthenium Alloy Electrodes," *J. Electrochem. Soc.*, **138**, 1321 (1991).

44. Janssen, M.M.P., and Moolhuysen, J., "Platinum-Tin Catalysts for Methanol Fuel Cells Prepared by a Novel Immersion Technique, by Electrocodeposition and by Alloying," *Electrochim. Acta*, **21**, 861 (1976).

45. Janssen, M.M.P., and Moolhuysen, J., "State and Action of the Tin Atoms in Platinum-Tin Catalysts for Methanol Fuel Cells," *J. of Catal.*, **46**, 289 (1977).

46. Watanabe, M., Furuuchi, Y., and Motoo, S., "Electrocatalysis by Ad-atoms. Part XIII. Preparation of Ad-electrodes with Tin Ad-atoms for Methanol, Formaldehyde and Formic Acid Fuel Cells," *J. Electroanal. Chem.*, **191**, 367 (1985).

47. Norton-Haner, A.N., and Ross, P.N., "The Electrochemical Oxidation of Methanol on Sn-Modified Pt Single-Crystal Surfaces," *J. Phys. Chem.*, **95**, 3740 (1991).

48. Ross, P.N., and Norton-Haner, S., "The Chemistry of Methanol Electrooxidation on Pt_3Sn Single Crystal Surfaces," LBL communication (1990).

49. Janssen, M.M.P., and Moolhuysen, J., "Binary Systems of Platinum and a Second Metal as Oxidation Catalysts for Methanol Fuel Cells," *Electrochim. Acta*, **21**, 869 (1976).

50. Beden, B., Kadirgan, F., Lamy, C., and Leger, J.M., "Electrocatalytic Oxidation of Methanol on Platinum-Based Binary Electrodes," *J. Electroanal. Chem.*, **127**, 75 (1981).

51. Shibata, M., and Motoo, S., "Electrocatalysis by Ad-Atoms: Part XX—Rate-Determining Step in Methanol Oxidation Enhanced by Oxygen-Adsorbing Ad-Atoms," *J. Electroanal. Chem.*, **209**, 151 (1986).

52. Hamnett, A., Kennedy, B.J., and Wagner, F.E., "Pt-Ru Anodes for Methanol Electrooxidation: A Ruthenium-99 Mössbauer Study," *J. Catal.*, **124**, 30 (1990).

53. McNicol, B.D., and Short, R.T., "Short Communication: The Reducibility of Ru, Pt/Ru and Pt Oxide Electrocatalysts as Measured by Temperature-Programmed Reduction and Cyclic Voltammetry," *J. Electroanal. Chem.*, **92**, 115 (1978).

54. McNicol, B.D., and Short, R.T., "The Influence of Activation Conditions on The Performance of Platinum/Ruthenium Methanol Electro-Oxidation Catalysts. Surface Enrichment Phenomena," *J. Electroanal. Chem.*, **81**, 249 (1977).

55. Gasteiger, H.A., Ross, P.N., Cairns, E.J., Work in progress, June 1992.

56. Kinoshita, K., and Stonehart, P., "Preparation and Characterization of Highly Dispersed Electrocatalytic Materials," *Modern Aspects of Electrochemistry, v. 12*, (1977) p. 183.

57. Schwartz, D.T. and Müller, R.H., "Oxidation Films on Copper IN Alkaline Media: Intensity Modulated Photoelectrochemical and Raman Spectroscopy Studies," *Surf. Sci.*, **248**, 349 (1991).

58. Mayer, S.T. and Müller, R.H., "An *In Situ* Raman Spectroscopy Study of the Anodic Oxidation of Copper in Alkaline Media," *J. Electrochem. Soc.*, **139**, 426 (1992); Mayer, S.T., Ph.D. Thesis, University of California, Berkeley, CA (1989); Lawrence Berkeley Laboratory Report LBL-15607.

59. Chieu, T.C., and Dresselhaus, M.S., "Raman Studies of Benzene-Derived Graphite Fibers," *Physical Review* B, **26**, 5867 (1982).

60. Tuinstra, F., and Koenig, J.L., "Characterization of Graphite Fiber Surfaces with Raman Spectroscopy," *J. Composite Materials*, **4**, 492 (1970).

61. Ager, J.W. III, Veirs, D.K., Shamir, J., and Rosenblatt, G.M., "Laser Heating Effects in the Characterization of Carbon Fibers by Raman Spectroscopy," *J. Appl. Phys.*, **66**, 3598 (1990).

62. Cairns, E.J., "Some Physicochemical Properties of Aqueous Fluoride- and Cesium-Containing Electrolytes," *Electrochem. Tech.*, **5**, 8 (1967).

63. Striebel, K.A., McLarnon, F.R., and Cairns, E.J., "Oxygen Reduction on Pt in Aqueous K_2CO_3 and KOH," *J. Electrochem. Soc.*, **137**, 3351 (1990).

64. Striebel, K.A., McLarnon, F.R., and Cairns, E.J., "Fuel Cell Cathode Studies in Aqueous K_2CO_3 and KOH," *J. Electrochem. Soc.*, **137**, 3360 (1990).

65. Striebel, K.A., "Oxygen Reduction in Fuel Cell Electrolytes," PhD Thesis (1987); also, Lawrence Berkeley Laboratory Report LBL-24340.

66. Cullity, B.D., *Elements of X-Ray Diffraction, Second Edition*, Addison-Wesley Publishing Company, Inc. (1978).

67. Ross, P.N., "Review Article: Characterization of Alloy Electrocatalysts for Direct Oxidation of Methanol: New Methods," *Electrochimica Acta*, **36**, 2053 (1991). Also, Ross, P.N., "Characterization of Alloy Electrocatalysts for Direct Oxidation of Methanol," LBL Report (1991).

68. Kinoshita, K., and Ross, P.N., "Oxide Stability and Chemisorption Properties of Supported Ruthenium Electrocatalysts," *J. Electroanal. Chem.*, **78**, 313 (1977).

69. Ticanelli, E., Beery, J.G., Paffett, M.T., and Gottesfeld, S., "An Electrochemical, Ellipsometric, and Surface Science Investigation of the PtRu Bulk Alloy Surface," *J. Electroanal. Chem.*, **258**, 61 (1989).

70. Stonehart, P., "Development of Advanced Noble Metal-Alloy Electrocatalysts for Phosphoric Acid Fuel Cells (PAFC)," *Ber. Bunsenges. Phys. Chem.*, **94**, 913 (1990).

71. Landsman, D.A., and Luczak, F.J., "Investigation of the *In situ* Oxidation of Methanol in Fuel Cells," Prepared for U.S. Army Mobility Equipment Research and Development Command, Fort Belvoir, VA by United Technologies Power Systems (1981).

72. Goodenough, J.B., Hamnett, A., Kennedy, B.J., Manoharan, R., and Weeks, S.A., "Porous Carbon Anodes for the Direct Methanol Fuel Cell--I. The Role of the Reduction Method for Carbon Supported Platinum Electrodes," *Electrochim. Acta*, **35**, 199 (1990).

73. Hamnett, A., Weeks, S.A., Kennedy, B.J., Troughton, G., and Christensen, P.A, "Long-Term Poisoning of Methanol Anodes," *Ber. Bunsenges. Phys. Chem.*, **94**, 1014 (1990).

Appendix A. Electrode Parameters

Listed in Table A-1 are the physical parameters of the gas diffusion electrodes fabricated in-house. Included are name of the electrode (for reference purposes), type of catalyst, metal loading in the reaction layer, PTFE content of the reaction layer, and PTFE content of the gas diffusion layer. For the composition column, C refers to amorphous, high-surface-area carbon substrate (Vulcan XC-72R), and G refers to graphitized high-surface-area carbon. Those catalysts made with Pt-Ru have a Pt:Ru atomic ratio of 1:1, and were loaded on the graphitized carbon substrate as 5 w/o total metal content, unless otherwise noted. All electrodes had a reaction layer of 20 cm^2, supported on a gas diffusion layer, which was 30 cm^2, made from wet-proofed TGP-120H (Toray, Co.) graphite paper.

Table A-1. Physical parameters for the fabrication of gas diffusion electrodes

Num.	Compo-sition	Loading (mg/cm^2)	PTFE in RL (w/o)	PTFE in GDL (w/o)	Comments
17	Pt/C	1.5	25	43	Prototech catalyst, 10% Pt/C; pressing @ ≤500lb; used woven Pellon instead of Celgard.
21	Pt/Ru/G	0.5	30	45	10% Pt-Ru/G (C-4); low pressures; Pellon.
23	Pt/Ru/G	0.5	30	46	Same as 21.
25	Pt/Ru/G	0.5	30	47	Same as 21.
26	Pt/G	0.5	30	47	10% Pt/G (C-1); same press as 21.
28	Pt/Ru/G	0.5	4.1	46	Should be 25 % PTFE in RL. Never tried polarization curves, though it might be interesting.
29	Pt/Ru/G	0.5	20	47	Same as 28; sticking to Pellon
36	Pt/Ru/G	0.5	20	60	1st electrode pressed w/ Celgard; dramatic improvement.
37	Pt/Ru/G	0.5	10	60	Same as 36; cut in half: 1 sintered in tube furnace (pass), 1 on press (fail).
40	Pt/Ru/G	0.5	15	54	Same as 36.
41	Pt/Ru/G	0.5	15	52	Same as 36; pressures taken up to 5000 lbs during sinter.
42	Pt/Ru/G	0.5	10	52	Same as 41; 1st use of copy paper
43	E-TEK[12]	0.5	15	52	Same as 43.
45	Pt/Ru/G	0.5	40	56	Same as 43.
46	Pt/Ru/G	0.5	30	55	Same as 43; no shim on sintering.
48	Pt/Ru/C	0.5	30	50	Same as 46.
49	Pt/Ru/G	0.5	20	51	Same as 46.
50	Pt/G	1.0	20	49	Same as 46. 10% Pt/G (C-10)

[12]Supplied bky E-TEK Inc. (Framingham, MA).

Appendix B. Fabrication of the Gas Diffusion Electrode

Preparing the gas diffusion layer 80
Preparing the reaction layer 81
Putting the reaction layer onto the gas diffusion layer 81
Pressing the Electrode 83

Preparing the gas diffusion layer

- Cut graphite paper to size (5 cm by 6 cm) and weigh. Record this as the initial weight of the gas diffusion layer, W_i.
- Pour 5 ml of DI water into a 5-inch crystallization dish, then add 15 ml of FEP-120 PTFE suspension (DuPont) (to make a three-fourths dilution). Gently mix.
- Place graphite paper flat into Teflon and, making sure it is completely covered, soak for 10 minutes.
- Remove graphite paper and lightly blot on lint-free cloth to remove excess liquid.
- Dry in oven 30 minutes at 90 °C. Note: do not lay paper flat on oven shelf; prop it up.
- "Cure" the paper in a muffle furnace at 335 °C for 15 minutes, let cool, and weigh; record weight as W_f.

- Calculate the weight percent of FEP in the gas diffusion layer and record: $W_{TFE} = \frac{W_f - W_i}{W_i}$.

Preparing the reaction layer

- Measure out catalyst required:

$$W_{cat} = \frac{1}{L_{cat}} \text{ X } L_{elec} \text{ X } A_{elec}$$

For example, for 0.5 mg [total metal]/cm^2 using 5 w/o metal on carbon (0.5 mg metal per mg of catalyst) and 20 cm^2 electrode area one would use 200 mg of catalyst.

- Place approximately 3 ml of water into a small beaker plus a small drop of surfactant (Triton X-100).
- Pour the catalyst into the water and allow the catalyst to wet completely.
- Mix the catalyst-water mixture with an ultrasonic agitator (Vibracell) until a thick slurry is formed. Continue adding small amounts of water while mixing until the slurry is thin enough to pour, for 200 mg of catalyst this will give a total volume of approximately 20 ml. **Caution**: do not thin out the mixture with too much water; this will cause the catalyst slurry to pull completely through the gas diffusion layer during the vacuuming steps. A slurry which is too thin will have the characteristics of a thin paint.

Putting the reaction layer onto the gas diffusion layer

- Place the gas diffusion layer onto a wetted sheet of filter paper centered on the steel meshes on the vacuum table (see Figure B-1).

- Wet the mesh and the plastic rim of the vacuum table thoroughly. This will help maintain a good seal for the vacuum.
- Center the rubber mask over the gas diffusion layer.
- Place the plastic and aluminum pressure-plates over the rubber mask and secure tightly by bolting the aluminum frame-plate to the vacuum table.
- Pour the reaction layer slurry into the well formed by the pressure plates and the rubber mask. Slightly agitate the vacuum table to ensure that the slurry is evenly distributed over the surface of the gas diffusion layer.
- Turn on the vacuum. The vacuum line should go through a Ehrlenmayer vacuum flask to trap liquids. Partially cover the side-arm hole on the flask with a finger and slowly increase the coverage over the hole to increase the vacuum until the water begins to be pulled from the reaction layer and through the gas diffusion layer. Keep the rate slow and steady to uniformly dry the reaction layer.
- When the reaction layer looks mostly dry, but **before** cracks begin to appear, release the vacuum by removing your finger from the flask side-arm.
- Remove the aluminum and plastic pressure plates. Care should be taken when lifting the plastic plate from the rubber mask; the rubber mask will adhere to the plastic, so a spatula or other thin, flat object should be inserted between the two to break the seal. Carefully peel up the rubber mask and remove the electrode assembly.

Pressing the Electrode

The procedure for pressing the electrode assembly is outlined in Table B-1, which outlines the parts required for each pressing-step. The electrode assembly was placed in a hydraulic press equipped with heated platens with items in the order depicted in Figure B-1. The shims were strips of brass or steel cut from stock sheet metal. The absorbent layers were cut from stock copy machine paper (very smooth surface). Celgard (Celanese Co.) is a microporous polypropylene film, which easily transports water from the electrode surface, has a very smooth finish, and comes away from the surface without significant peeling. A highly absorbant cloth (Texwipe,) was used beneath the gas diffusion electrode to absorb water transported through the gas diffusion layer during pressing. The aluminum foil was used during the sintering step. An envelope was formed with the foil, the electrode (having been dried at 295 °C) was placed in the envelope, and the envelope was purged several times with nitrogen to reduce the volume of oxygen and consequently minimize oxidation of the carbon substrate during sintering. Additionally, a "sacrificial" layer of foil was placed between the envelope and each of the heated platens to prevent sticking. For the last pressing step, the platens were pre-heated to the desired temperature (note: this takes approximately 3 hours).

Between each of the first seven steps, any absorbant materials (*i.e.*, Texwipes or copy paper, if applicable) were replaced with fresh material. The polypropylene film was not disturbed until after drying in the oven at 90 °C, at which time the film was mostly self-detached. The pressing time for the first eight steps was not critical, but ranged from three to five minutes to remove water as efficiently as possible. For the sintering step, the electrode

was pressed for exactly fifteen minutes. Normally, the aluminum foil easily separated from the electrode; however, if there was strong adhesion and the risk of peeling, the electrode and foil were placed in concentrated potassium hydroxide to dissolve the foil.

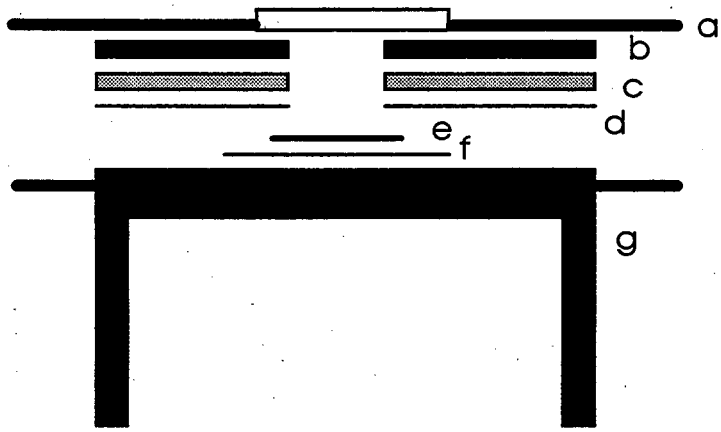

Figure B-1. Vacuum table assembly. a) Hold-down bracket; b) aluminum frame; c) plexiglass frame; d) rubber mask; e) gas diffusion layer of the electrode; f) filter paperl; g) vacuum table base.

Table B-1. Parameters for pressing and sintering the gas diffusion electrode assembly[13]

Press step	1	2	3	4	5	6	7	8	9
Shims (mils)	32	32	18	18	18	18	none	none	none
Absorbant Layers	2	2	1	1	1	1	1	none	none
Cellgard?	Y	Y	Y	Y	Y	Y	Y	Y	N
Texwipe?	Y	Y	Y	N	N	N	N	N	N
Al Foil?	N	N	N	N	N	N	N	N	Y
Temp (°C)	R.T.	R.T.	R.T.	R.T.	R.T.	R.T.	R.T.	R.T.	350
Pressure (lbs ga.)	slight	1000	2000	3000	3000	5000	1000	5000	5000
Pressure (kg/cm^2)	slight	23	45	68	68	114	23	114	114

[13]Between steps 8 and 9, the electrode assembly is removed from the press, dried in an oven at 90 °C for approximately 30 min., then placed in a furnace at 295 °C for 30 min. to burn off wetting agents used in the TFE-30 solution.

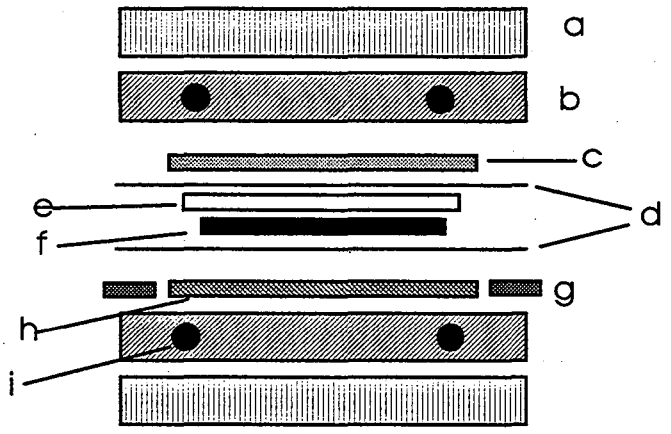

Figure B-2. Assembly order for the press and electrode parts. a) ceramic insulators; b) heated brass platens; c) absorbant paper; d) aluminum foil; e) Cellgard (polypropylene film); f) gas diffusion electrode, reaction layer side up; g) shims; h) Texwipe absorbant cloth; i) holes for heating cartridges. Note: not all parts will be used at the same time; see Table B-1 for details.

LAWRENCE BERKELEY LABORATORY
UNIVERSITY OF CALIFORNIA
TECHNICAL INFORMATION DEPARTMENT
BERKELEY, CALIFORNIA 94720